2014•2015
FACULTEIT GENEESKUNDE EN LEVENSWETENSCHAPPEN
master in de biomedische wetenschappen

Masterproef

Ion beam doping and defect engineering of ZnO nanowires for photodetection and sensing applications

Promotor :
Prof. dr. Hans-Gerhard BOYEN

Promotor :
Prof.dr. CARSTEN RONNING

Michelle Geelen

Scriptie ingediend tot het behalen van de graad van master in de biomedische wetenschappen

De transnationale Universiteit Limburg is een uniek samenwerkingsverband van twee universiteiten in twee landen: de Universiteit Hasselt en Maastricht University.

universiteit hasselt
KNOWLEDGE IN ACTION

Universiteit Hasselt | Campus Hasselt | Martelarenlaan 42 | BE-3500 Hasselt
Universiteit Hasselt | Campus Diepenbeek | Agoralaan Gebouw D | BE-3590 Diepenbeek

universiteit hasselt | Maastricht University

2014•2015
FACULTEIT GENEESKUNDE EN LEVENSWETENSCHAPPEN
master in de biomedische wetenschappen

Masterproef

Ion beam doping and defect engineering of ZnO nanowires for photodetection and sensing applications

Promotor :
Prof. dr. Hans-Gerhard BOYEN

Promotor :
Prof.dr. CARSTEN RONNING

Michelle Geelen

Scriptie ingediend tot het behalen van de graad van master in de biomedische wetenschappen

universiteit hasselt | Maastricht University

Foreword

Learning about business: don't compete but dominate; success goes hand in hand with preparation…
Don't lower your goals, keep working hard and chase your dreams!

Dear reader,

In front of you is a report on the ion beam modification of zinc oxide nanowires for photodetection and sensing applications. This report is written as completion of the master Bioelectronics & Nanotechnology at the University of Hasselt. The research was executed as an internship at the Institut für Festkörperphysik in Jena (Germany). The aim of this research training was to perform individual scientific research in a research group in order to get more inside in the field of science. This involves the use of previously acquired knowledge, insight and skills.

This report looks at the electrical and photoconductivity properties of zinc oxide nanowires. The intent is to investigate the persistence of the photoconductivity, whose origin is still controversial. Ion implantation was used to manipulate the functionalities of both the electrical and synthesized nanowires. Introducing a small amount of other elements may lead to a modification of the photoconductivity properties of the nanowires. As a scientist, I wanted to find out what the opportunities and/or restrictions are for the use of ion implantation and the specific influence on the electrical and photoconductivity properties of ZnO nanowires.

The final report is the result of long days spent in the lab, battling shoulder to shoulder with my colleagues and friends, the hope for good results and the sadness with each failed attempt.

I wish you a pleasant read.

Michelle Geelen

Content

Abstract

The recent progress in science has led to a transition to the nano-world. Semiconducting systems such as ZnO nanowires have drawn a lot of interest for sensor applications, in particular chemical and biological sensing as well as photodetection. This is due to the astonishing surface-to-volume ratio and high sensitivity of the surface under ambient conditions. However, the integration of in particular ZnO nanowires has one major drawback, namely the persistence of the photoconductivity. Instead of quickly returning to the original level, the conductivity persists for several minutes or even hours after switching off the illumination. This effect, known as persistence of the photoconductivity, strongly depends on the properties of the nanowire surface, the doping and the environment conditions. Therefore, the modification of the surface properties, for example through doping procedure, can induce a change in the photoconductivity properties. Within the frame of this thesis, the effect of introducing a controlled amount of aluminum into the crystal lattice of ZnO by means of ion beam implantation was examined. Although aluminum is known to act in ZnO as n-type donor, the implantation process generates additionally defects within the crystal, which can also influence the electrical and photoconductivity properties of ZnO nanowires. Therefore, additional implantation with argon ions was considered as a reference, in order to separate the effect of defects and the aluminum dopants.

More insight in the underlying physical processes was obtained by investigating the electrical properties of the ZnO nanowires. ZnO nanowires were synthesized using the vapor-liquid-solid growth mechanism. They were then transferred onto a clean Si/SiO_2 substrate and assembled into a field-effect-transistor configuration by photolithography. The electrical and photoconductivity properties of the produced devices were investigated before and after implantation. The as-implanted samples were found to be highly isolating due to the presence of defects generated during implantation. Thermal annealing at 300 °C has shown that the defect concentration can be reduced. The annealing acts also as activator for the introduced n-type dopants and gave rise to enhancement of the photoconductivity. Furthermore, aluminum implantation causes an increase of the persistence of the photoconductivity. After the electrical characterization, photoluminescence measurements were performed, in order to confirm the successful activation of aluminum in ZnO nanowires.

In conclusion, by intentionally adding aluminum to the lattice one can manipulate the functionalities of ZnO nanowires. The results of this study lead to a better understanding of the fundamental procedures. This may result in a more effective way of designing new nanodevices for commercial applications, such as for chemical or biological sensing.

Samenvatting

De recente evolutie in wetenschap en onderzoek heeft aanleiding gegeven tot de transitie naar de nano-wereld. Semiconductors zoals ZnO nanowires hebben de interesse gewekt van wetenschappers voor sensor applicaties, voornamelijk gas sensing en fotodetectie. Dit is te wijten aan hun uitzonderlijke surface-to-volume ratio en gevoeligheid onder omgevingsomstandigheden. De integratie van ZnO nanowires in commerciële toepassingen heeft een belangrijk nadeel, namelijk de persistentie van de photoconductiviteit. Na het uitschakelen van UV licht, behoudt de photocurrent zijn verhoogde niveau gedurende minuten of zelfs uren vooraleer terug te keren naar het originele niveau. Dit effect, beter bekend als "persistence of the photoconductivity", is sterk afhankelijk van de oppervlakte eigenschappen van de nanowire, de doping en de omgevingsomstandigheden. Om deze reden kan modificatie van de oppervlakte eigenschappen, door gebruik te maken van doping procedures, veranderingen teweegbrengen in de fotoconductiviteit. In het kader van deze thesis, werd het effect bestudeerd van de introductie van aluminium in het ZnO kristal met behulp van ion beam implantation. Hoewel bekend is dat aluminium fungeert als n-type donor in ZnO, genereert het implantatie proces aanvullend defecten in het kristal. Deze bijkomende defecten kunnen de elektrische eigenschappen en de fotoconductiviteit van ZnO nanowires beïnvloeden. Om een onderscheid te maken tussen de invloed van defecten en aluminium dopants, werd implantatie met argon ionen beschouwd als referentie.

Meer inzicht in de onderliggende fysische processen werd verkregen door het bestuderen van de elektrische eigenschappen van de ZnO nanowires. ZnO nanowires werden gesynthetiseerd door gebruik te maken van het vapor-liquid-solid groei mechanisme. Vervolgens werden de nanowires overgebracht op een proper Si/SiO_2 substraat en samengesteld in een field-effect-transistor configuratie met behulp van fotolithografie. De elektrische en fotoconductiviteit eigenschappen van de vervaardigde toestellen werd onderzocht voor en na implantatie. De geïmplanteerde stalen waren sterk isolerend als gevolg van de aanwezigheid van defecten, gegenereerd tijdens de implantatie. Thermal annealing op 300 °C heeft aangetoond dat de defect concentratie gereduceerd kan worden. De annealing fungeert als activator voor de geïntroduceerde n-type dopants en geeft aanleiding tot versterkte fotoconductiviteit. Verder veroorzaakt aluminium implantatie een stijging van de persistentie van de fotoconductiviteit. Na het voltooien van de elektrische karakterisatie werden fotoluminescentie metingen uitgevoerd voor het bevestigen van de succesvolle aluminium activatie in ZnO nanowires.

Het opzettelijk toevoegen van aluminium aan het lattice kan gebruikt worden voor het manipuleren van de functies van ZnO nanowires. De resultaten van deze studie leiden tot een beter begrip van de fundamentele processen. Dit kan resulteren in een effectievere manier om nieuwe nanodevices te ontwerpen voor commerciële toepassingen, zoals chemische of biologische sensing.

Abbreviations

DLE	Deep Level Emission
EBIC	Electron Beam Induced Current
E_F	Fermi level
FET	Field-Effect-Transistor
FX	Free Exciton
I-V	Current-Voltage
LED	Light Emitting Diode
LO	Longitudinal Optical
NBE	Near-Band-Edge
PL	Photoluminescence
PPC	Persistent Photoconductivity
sccm	Standard cubic centimeters per minute
SEM	Scanning Electron Microscopy
SMU	Source-Measure Unit
SRIM	Stopping and Range of Ions in Matter
SX	Surface Exciton
TES	Two-Electron Satellite
UV	Ultraviolet
VLS	Vapor-Liquid-Solid
ZnO	Zinc Oxide

1 Introduction

In the last decades electronic devices have found their way into many areas of society, ranging from domestic appliances that wake us in the morning to high technology communication systems and medical instruments [1,2]. Our way of life has led to an evolution in biology and technology and to the development of bio-electronics. This field combines the study of the micro- and nanobiotic world with progressively smaller electronic circuits [3].

By shrinking down to molecular and atomic levels we enter a new world. The term nanotechnology, introduced for the first time by Professor Norio Taniguchi in 1974, refers to the development of man-made devices with a specific function by controlling the size on the nanometer length scale [4]. These materials exploit novel properties and phenomena that can significantly vary when structural parameters such as size and shape are altered [5].

The interdisciplinary nature of the word 'nano' is apparent in the manufacturing of nanostructures [6]. By scaling down, it is possible to fine-tune materials to favored properties [7]. Top-down approaches create products by reducing the size of large pieces of matter. However, this method is reaching its limits due to the encounter with quantum mechanics and wave optics [8]. An alternative route is called bottom-up fabrication. This approach relies on self arrangement processes similarly used nature to create biological systems. Atoms and molecules are used as building blocks for self-organization into the desired structures. The more insight is gained into the involved processes, the more interesting and powerful nanostructures appear.

Low-dimensional systems, such as nanotubes, nanobelts and nanowires, have attracted significant interest in several fields such as for instance electronics, photonics and medical sciences [9,10]. Nanowires are solid structures with at least one dimension in the nanometer range. They are often referred to as one-dimensional materials as a result of their large aspect or length-to-width ratio. Depending on the material components, the nanowire can behave as a metal, insulator or semiconductor. Semiconducting nanowires have drawn a lot of interest as ideal building blocks for nanoscale devices [11]. Due to the high surface-to-volume ratio they are particularly sensitive to environmental conditions and are therefore ideal candidates for sensing applications. Among semiconductor nanowires, metal oxide nanowires are an important class of functional materials, which have a wide range of application for transistors [12], light-emitting devices [13] and sensors [14]. The reason for this is their selectivity, stability and sensitivity, key parameters for high quality gas sensors [15]. One of the most widely used metal oxides is zinc oxide (ZnO). It is biocompatible, biodegradable and biosafe. In addition, its conductivity can be easily influenced by the surrounding surface properties [16]. These features, combined with the reduced production costs, are fundamental for efficient photodetection and ensure that these sensors can be applied in different fields [17].

Despite the abundant research on ZnO nanowires, their integration for photodetection applications is limited by the presence of persistent photoconductivity. In order to explore the possibilities for

future applications, it is important to study the fundamental properties in more detail to clarify the origin of this phenomenon. The optical and electrical properties can be affected by adding other elements to the crystal. However, the contribution of defects and dopants to the photoconduction is challenging to understand. Although a number of articles are published on the influence of UV illumination on the gas sensing performance, the detection mechanism is still controversial. A better understanding of the surface related processes and the role of defects and dopants may result in a more effective way of designing new devices for commercial application.

This thesis reports on the effect of introducing a controlled amount of aluminum into the crystal lattice of ZnO by means of ion beam implantation. Additional implantation with argon ions was considered as a reference, in order to separate the effect of defects and the aluminum dopants. More insight in the underlying physical processes was obtained by investigating the electrical properties of the ZnO nanowires before and after implantation, in particular the impact on the UV photoresponse increase and the dynamics of the photocurrent decay. SEM images were used for the determination of the changes in morphology after implantation and electrical characterization. In addition, the thermal stability of the electric properties was investigated since annealing may influence the electrical properties of the nanowires. The correlation between the electrical properties and the induced defects and dopants was further investigated by performing PL measurements on exact the same ZnO nanowires. Therefore, this research aims to contribute to a better understanding of the fundamental procedures. This may lead to the development of nanodevices in a better and more effective way with improved performance.

2 Background

2.1 Principles of semiconductors

Materials may be divided into conductors, semiconductors or insulators depending on the ability to conduct electric current under an external electric field. The classification is based on the properties of the valence electrons, which are involved in the chemical bonds between the lattice atoms [1]. These electrons contribute to the determination of the electrical properties of the crystal.

The difference between metals, semiconductors and insulators can be explained by their band model, as shown in figure 1. The higher band is called conduction band, while the lower band is known as the valence band. Electrons located in the conduction band are free and completely delocalized in the crystal, while electrons in the valence band are localized to the atomic sites and do not contribute to the conductivity. The two energy bands are separated by the bandgap (E_g), also known as the forbidden region. This value corresponds to the minimum energy required to excite electrons to the conduction band where they can contribute to the conductivity [18]. The band model includes also a thermodynamic quantity, namely the Fermi level (E_F). This term refers to the level where the probability of being occupied is equal to 50%.

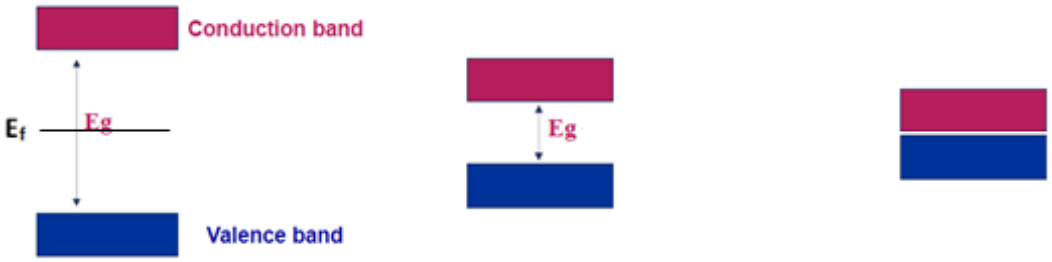

Figure 1: Band model of solid materials.
The schematic representation of the band model consists of a conduction band and a valence band separated by the bandgap (E_g). The Fermi level (E_F) corresponds to an occupation level of 50%.

Semiconductors are defined as materials with electrical properties between those of conductors, without any band gap and insulators, which are characterized by a wide band gap in the order of some eV. At low temperature, electrons have not enough energy to breach the energy gap, resulting in insulating behavior. As the temperature rises, thermal vibration of the crystal allows electrons to escape from their bonds and to be promoted to the conduction band, leaving a hole in the valence band. In semiconductors, the density of electrons in the conduction band or holes in the valence band can be increased by adding specific impurities into the crystal. This procedure is known as doping of semiconductors. When the doping process induces an excess of free electrons (holes), it is called n-type (p-type) doping. Further details about n-type and p-type doping will be given in section 2.5.

2.2 Metal - Semiconductor interface

Semiconductor devices for electronic and optoelectronic applications often include a metal-semiconductor interface. Therefore, the electrical properties of such devices depend not only on intrinsic parameters of the semiconductor but also on the contact between the semiconductor and the metallic electrode. The current (I) flowing across the metal-semiconductor interface will not always be linearly proportional to the applied bias voltage (V). This leads to asymmetric or rectifying current-voltage (I-V) characteristics.

When metal and semiconductor are in contact, electrons can move due to the difference in work function. If the metal work function is higher than that of the semiconductor, electrons in the conduction band are able to lower their energy by flowing from the semiconductor into the metal. This electron flow continues till both Fermi levels are aligned, leading to deformation of the band structure near the interface, as shown in figure 2. The barrier height ϕ_B is proportional to the difference between the metal work function ϕ_m and the semiconductor electron affinity χ_{SC} [19]:

$$\phi_B = \phi_m - \chi_{SC} \ .$$

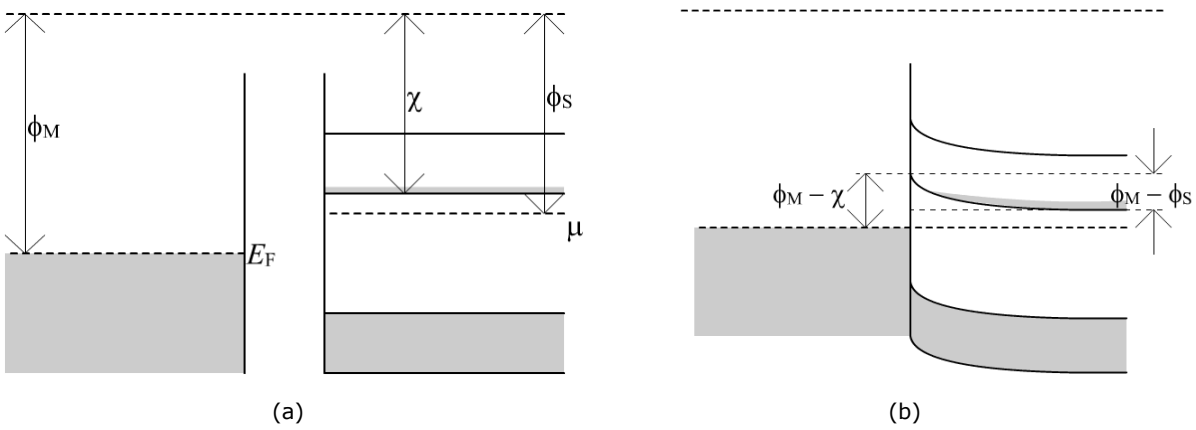

Figure 2: Band diagram of a metal-semiconductor junction.
When $\phi_m > \phi_s$, electrons flow from the semiconductor into the metal, until the Fermi levels are aligned. The diffusion results in the deformation of the band structure near the interface. Such junction is called a Schottky contact. Both images are adapted from [19].

The current flowing across a Schottky junction under an external voltage difference shows an exponential dependence on the voltage difference and is given by [20]:

$$I = A^* T^2 e^{-\frac{e\Phi_B}{kT}} \left(e^{-\frac{e\Delta V}{kT}} - 1 \right) ,$$

where A* is the Richardson constant, k is the Boltzmann constant, T is the absolute temperature and ΔV the applied potential.

However, the actual dependence of the barrier height on the work function is much lower than the prediction introduced by Schottky and Mott [21]. This insensitivity to the metal work function is known as Fermi level pinning. Due to the presence of metal-induced gap states, caused at the

semiconductor-metal junction by e.g. dangling bonds, the Fermi level is pinned to the center of the band gap [21]. When the barrier is sufficiently high, the electrons flow from the semiconductor to the metal. This diffusion results in the formation of a depletion zone near the interface [20]. This results in the rectifying behavior of the I-V characteristics.

In case of n-type semiconductors, when $\phi_m - \chi_{SC}$ is smaller than 0, the I-V characteristics are linear. Such a contact is referred to as ohmic.

2.3 Properties and applications of zinc oxide

In the scope of this thesis, experiments have been performed with semiconductor nanowires made of ZnO. ZnO received broad research attention since its rediscovery in the 1950s [22]. Although ZnO is chemically synthesized, it occurs naturally in the form of zincite.

ZnO is an II-VI semiconductor material which is available in various growth architectures, ranging from nanowires, nanoflowers to nanosprings etc. Owing to its direct wide bandgap (Eg = 3,37 eV) at room temperature, ZnO is regarded as a key material that can operate in the ultraviolet (UV) range. ZnO is n-type doped due to the presence of intrinsic oxygen vacancies [23]. One of the advantages of ZnO over other semiconductors is the large exciton binding energy (~60 meV). This will ensure efficient luminescence and bright exciton emission at room temperature [24].

ZnO belongs to the family of hexagonal wurtzite structures, shown in figure 3 [25]. The structure is composed of alternating planes of oxygen anions and zinc cations. Every oxygen atom is surrounded by four atoms of zinc in the form of a tetrahedral unit and vice versa [26]. The planes are stacked along the c-axis.

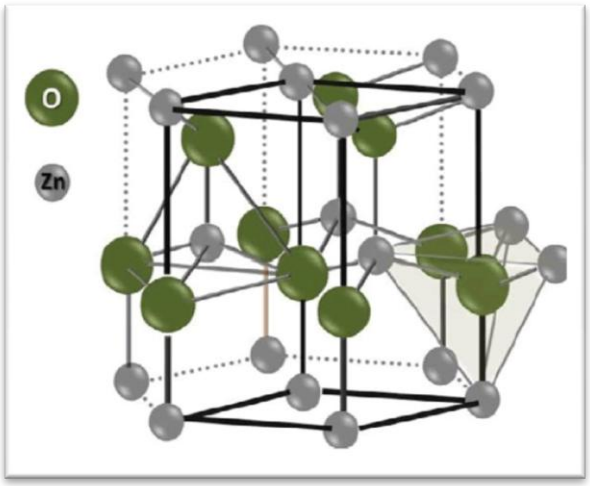

Figure 3: Representation of the wurtzite structure of ZnO.
The crystal structure of ZnO is characterized by a hexagonally packed lattice. Each oxygen anion is surrounded by four zinc cations forming a tetrahedron. The grey and green spheres denote Zn and O atoms, respectively. Image adapted from [25].

Despite the fact that nanotechnology is already widely used in experimental research, there are also applications in our daily lives. ZnO is used for instance as inorganic sun blocker, protecting the skin from sunburn by absorbing UV-A and UV-B radiation [27]. In addition, the ZnO ensures that the sunlight is scattered away from the skin.

Due to the lack of symmetry and its strong ionic character, the ZnO structure displays some unique properties, for example piezoelectricity. The term piezoelectricity refers to the electromechanical behavior of the material. By placing crystals with polar surfaces in an electric field, mechanical energy is converted into electrical energy. This behavior is important in the development of resonators and piezoelectric sensors [24]. But it has also applications in the exciting field of nanopiezotronics for harvesting energy and converting it into electricity [28,29]. The control of the morphology makes ZnO nanowires also candidates for nanogenerators, UV lasers, and other optoelectronic devices. The features described above and the fact that ZnO nanowires can be produced without much effort and cost makes it a promising material for future applications. Due to the reduced dimensions and their extraordinary surface-to-volume ratio they are highly influenced by their direct environment. Therefore, ZnO nanowires are dedicated to sensing, particularly biological and chemical sensing.

2.4 Surface properties of ZnO nanowires

The surface of a semiconductor is characterized by incomplete covalent bonds due to the absence of lattice symmetry. These dangling bonds result in intrinsic surface states within the bandgap [20]. The surface states can act as donors or acceptors depending on their charge when occupied. Because of the high density of surface states, the Fermi level is pinned at the ZnO surface. When the states act as electron acceptor, the pinning of the Fermi level leads to an upward banding and the formation of a depletion region near the surface.

A deeper understanding of the underlying physical phenomena is obtained by investigating the optoelectrical properties. The crystal structure of ZnO is characterized by the presence of intrinsic defects such as oxygen vacancies at the surface. Additionally, extrinsic surface states can be formed due to the presence of adsorbates at the semiconductor surface. For instance, the adsorption of oxygen at the ZnO surface induces the formation of surface states, which can trap electrons from the conduction band [30]. This process is described by the following formula:

$$O_2\,(g) + e^- \rightarrow O_2^-\,(ad)$$

The parameters refer to molecular oxygen in gas phase $O_2(g)$ and oxygen in its adsorbed state $O_2^-(ad)$.

The adsorbed oxygen provides a negative charge at the surface and gives rise to the upward band bending depicted in figure 4, right. This reduces the cross section of the conductive channel. The depletion region is directly proportional to the surface density of trapped electrons. The more oxygen is present in the environment, the wider the depletion layer and the lower is the conductivity of a nanowire with a large surface-to-volume ratio [31].

2.5 Photoconduction in ZnO nanowires

When the ZnO nanowires are kept in the dark, oxygen molecules from the surrounding are chemisorbed on the wire surface as described in section 2.4. The conductivity in dark is determined by the non-depleted part of the wire.

Upon illumination of the surface with UV light with an energy equal or larger than the bandgap, electron-hole pairs are created as shown in figure 4, left [15]. During this process electrons are excited from the valence band to the higher energy levels forming the conduction band [32]. The radial electrical field caused by the adsorbed oxygen forces the photogenerated holes to migrate to the surface. The resulting spatial separation of electrons and holes enhances the lifetime of the generated electrons [33]. Desorption of the absorbed oxygen molecules takes place by recombination of the photo-induced holes and the trapped electrons, according to the following formula:

$$h + O_2^- (ad) \rightarrow 0_2 (g)$$

This neutralization process results in a decrease of the band bending and the depletion layer [34]. Correspondingly, the conductivity of the nanowire increases.

However, the application of low-dimension systems as a sensor has one major obstacle, namely the presence of persistent photoconductivity (PPC) after UV excitation [35]. Instead of directly returning to the dark level, the increased conductivity persists for several minutes or hours. The nature of the PPC is still controversial. Some authors claim that this phenomenon is related to oxygen vacancies which give rise to metastable bulk defects [36]. Others assign it to the spatial separation of charge carriers according to the mechanism mentioned above [37]. When the UV light is switched off, oxygen molecules can readsorb on the surface, to trap photogenerated electrons, resulting in photocurrent decay. However, with increasing charge trapped at the surface, the height of the band bending increases. Therefore, there are less electrons available to the oxygen from the atmosphere reducing electron trapping and the photodecay rate. This leads to the extraordinarily long persistence of the photoconductivity.

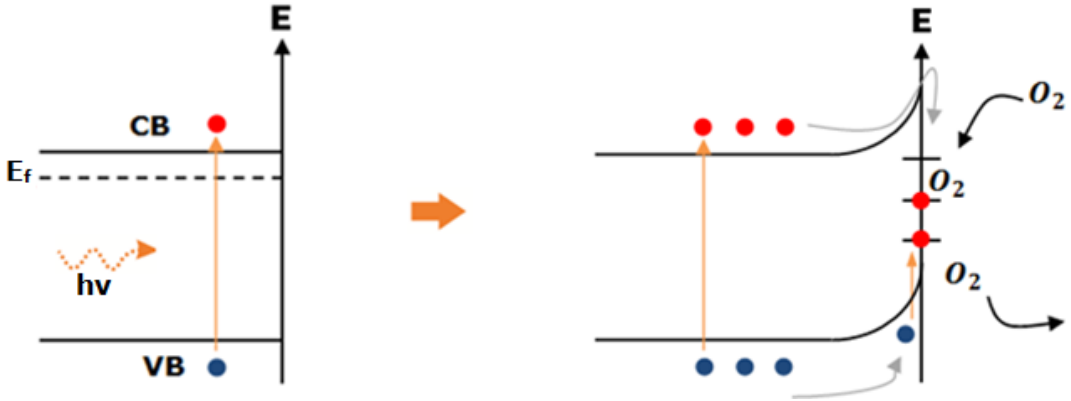

Figure 4: Band diagram of ZnO nanowire and its surface.
The image on the left shows the generation of electron-hole pairs after illumination. Due to band bending, the photogenerated holes can migrate to the surface. O_2 is chemisorbed by trapping of electrons from the conduction band as depicted on the right. This causes depletion of the electrons and a further upward bend bending. Recombination of trapped electrons and photo-induced holes leads to desorption of O_2. In both figures, the color of electrons is red, whereas the holes are blue.

2.6 Doping of ZnO nanowires

Enhanced control of the sensing device properties can be achieved by optimization of the nanowire surface. Possible modification techniques involve surface functionalization and doping. This has been practiced by the semiconductor industry since the production of sophisticated devices requires highly controlled properties. By intentionally adding a small amount of other elements to the lattice of a semiconductor one can manipulate the functionalities of the intrinsic material for enhanced application potentialities. There are two types of impurities, namely donors and acceptors as depicted in figure 5 in case of silicon. In case of n-type doping, one atom in the structure can be replaced by a pentavalent atom such as phosphorus. As a result, one unpaired electron floats around and gives rise to a higher Fermi-energy and thus a larger free electron concentration. In the case of p-type doping a trivalent atom such as boron is added to the lattice. This creates deficiencies in the number of electrons, called holes, whose concentration is therefore enhanced.

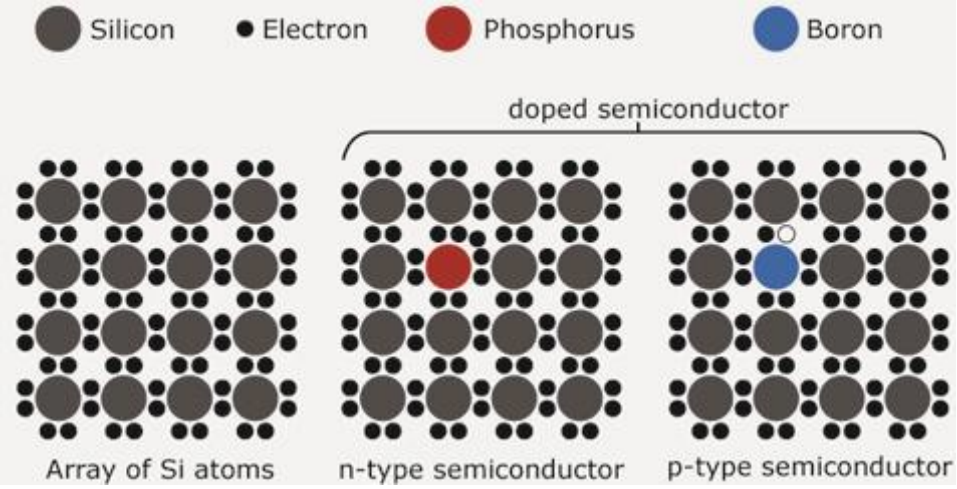

Figure 5: Mechanism of semiconductor doping.
Illustration of a silicon lattice doped with impurities to produce n-doped and p-doped semiconductors. Left: Schematic representation of an intrinsic silicon crystal. Middle: The addition of Phosphorus to the silicon lattice results in extra electrons. This gives rise to n-type semiconductors. Right: Representation of bonds a crystal doped with a trivalent atom such as boron. The presence of holes is typical for semiconductors. Image taken from [38].

Doping of semiconductors can be carried out by means of three different methods: doping during growth, diffusion and ion implantation. By supplying the dopant during growth, dopants can be incorporated into the crystal. However, controlled doping during growth of nanowires is an unsolved problem. The difficulties are due to the underlying processes involved in the Vapor-Liquid-Solid (VLS) growth mechanism. As this is a self-regulation process, there is little control over diffusion of dopants towards the surface and incorporation of unwanted elements [39].

Subsequent doping via diffusion is explored in less detail. The main process involves the diffusion of atoms according their concentration gradient. Due to the enhanced surface-to-volume ratio, nanowires are more sensitive for high temperatures required to induce the diffusion process. Therefore, this method is not convenient for one-dimensional structures [40].

An alternative route to dope semiconductors is ion implantation. This well-known industrial technique can incorporate a controlled amount of dopant ions with a reasonable control of the depth profile. As ion bombardment is a process far from thermal equilibrium, dopant concentrations beyond the solubility limit of principally every element are possible [40]. The ion radiation will however also induce unwanted damage in the structure and morphology of the target material. This can range from point defects to complete amorphization and material loss by sputtering [41]. This need not to be disadvantageous, as the defects can also be used for manipulation of the irradiated structures. Also they offer opportunities for the control of the morphology, namely the bending and the alignment of nanowires in the desired orientation [42].

3 Material and Methods

3.1 Synthesis of semiconductor nanowires

One of the most exploited methods to synthesize nanowires in a controlled way is the so-called VLS mechanism. This technique was first used in the 1960s by Wagner and Ellis for the growth of Silicon whiskers [43]. In this method a gold droplet is used as a catalyst. Deposition of source material in the vapor phase on the liquid catalyst results in a liquid alloy phase. When the concentration of the source material exceeds the supersaturation level, the material starts to segregate and recrystallize from which outward growth can occur [44]. The growth continues as long as the reactant is available. The diameter of the nanowire is in general defined by the size of the catalyst. The above described process is schematically illustrated in figure 6.

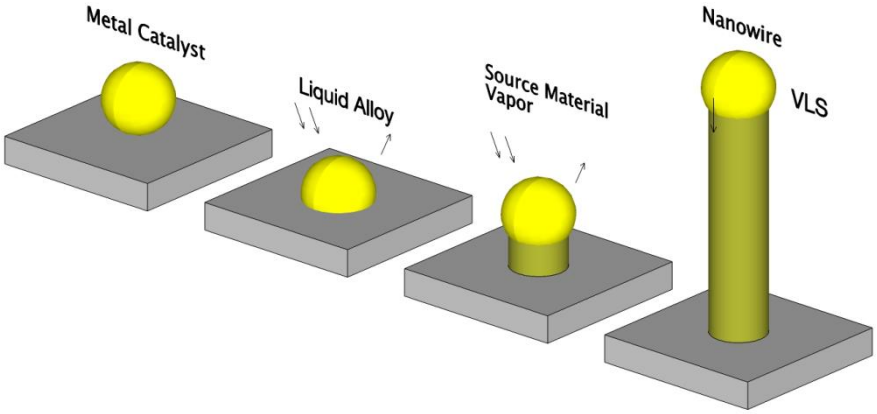

Figure 6: Growth of semiconductor nanowires using a gold catalyst.
The vapor liquid solid growth process is catalyzed by a gold layer deposited on the substrate. The gold layer is transformed into an eutectic alloy upon heating, which leads to axial growth beneath the droplet.

Silicon wafers with a 1000 nm thick SiO_2 layer were used as growth substrates. The wafers were broken in pieces of 5 mm × 10 mm along scratches made with a diamond tip and ultrasonically cleaned in acetone for 3 minutes. Prior to the growth process the substrates were coated with 10 nm of gold by sputtering (Jeol JFC 1200). The sputtering process was performed at a pressure of 8 Pa and a current of 20 mA.

The growth process was performed in a horizontal tube furnace, depicted in figure 7. As source material, 2 g of ZnO powder, provided by the company Alfa Aesar, were inserted in the centre of the furnace. The gold coated substrates were located downstream. After heating to 1350 °C, the evaporated ZnO is transported by an argon flow of 50 standard cubic centimeters per minute (sccm) to the target substrates to initiate growth of nanostructures. The pressure during growth was between 20 and 100 mbar. Typical growth was carried out for 1 hour at a temperature of 1350 °C.

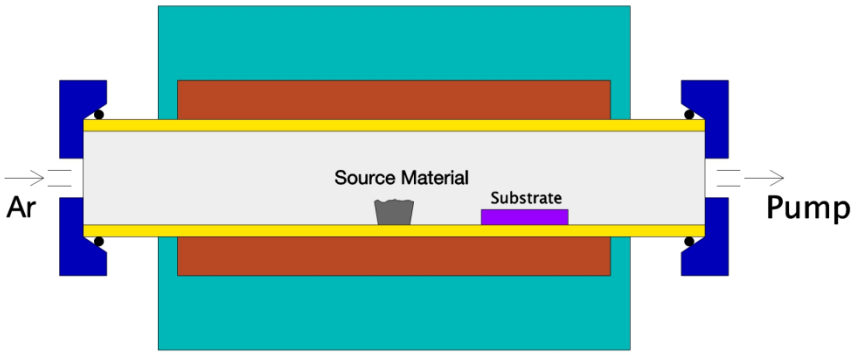

Figure 7: Schematic illustration of the experimental set-up for nanostructures growth.
The horizontal tube furnace contains a boat with source material. The target substrates are located more to the end of the set-up. By controlling the two heating elements surrounding the quartz tube a homogeneous growth can be achieved.

The morphological characterization of the as-grown nanowires was carried out by scanning electron microscopy (SEM). A typical image is shown in figure 8. The image shows ZnO nanowires grown on a silicon wafer coated with a 10 nm layer of gold. It can be seen that the wires are dispersively deposited over the entire surface area. The wires have rather uniform diameters of about 200 nm, which does not vary significantly along the length. Closer to the edge of the substrate are the wires shorter and not so pronounced. By adjusting the growth temperature and size of the catalyst, ensembles of aligned or fully randomly nanowires can be realized.

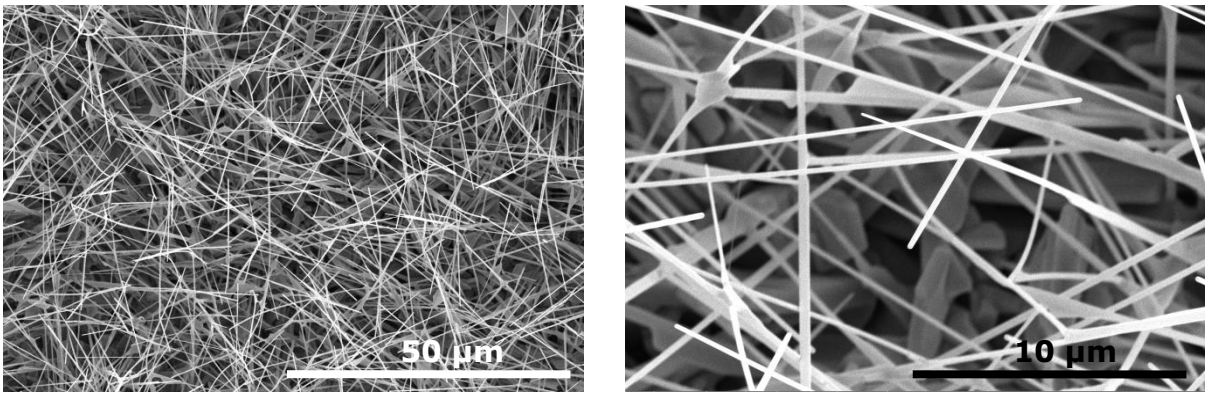

Figure 8: SEM images of ZnO nanowires.
SEM characterization of ZnO nanowires grown on silicon substrates at different magnifications, respectively 50 µm and 10 µm.

3.2 Contacting of nanowires

The synthesized ZnO nanowires were then assembled into a field-effect-transistors (FET) configuration. FETs have three terminals, which are called drain, source and gate, depending on their functions. In the so called back gate configuration, the gate electrode is located underneath the gate dioxide layer (figure 9). The current injected at the source flows through the nanowire to the drain. One is able to control the drain-source current flow by applying a voltage to the

gate [45]. The induced electric field controls the conductivity of the channel and hence the current flow. The processing steps required to produce the different contacts are described below.

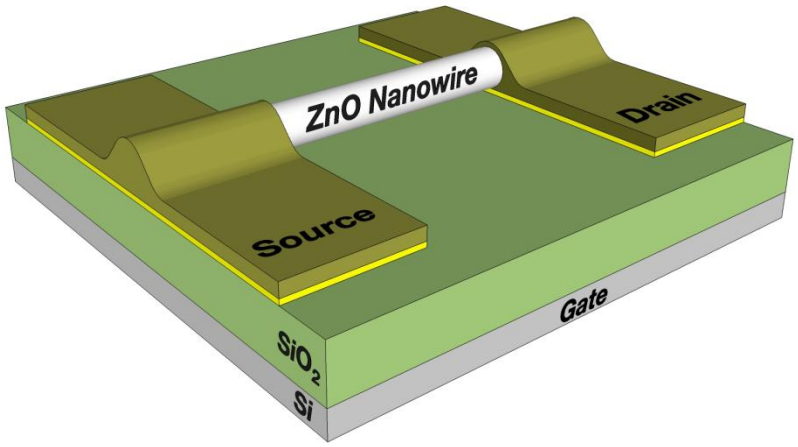

Figure 9: ZnO nanowire field effect transistor.
The top view of a FET shows how the channel, represented by the ZnO nanowire, is connected on both sides by the drain and source contacts. The underlying Si substrate can function as a gate by which one can control the current flowing between the contacts.

3.2.1 Imprinting

The grown nanowires are transferred onto a Si/SiO_2 substrate via dry contact imprinting. Slightly pressing the growth substrate in a preferential direction along the target substrate, results in the controlled alignment of the imprinted wires. By varying the applied force one is able to control the density of the transferred nanowires.

3.2.2 Lithography

In order to conduct electrical measurements, contacts have to be applied to the nanowires. These contact structures were predefined using UV photolithography. This technique is based on the transfer of geometrical patterns onto a substrate by means of UV irradiation. By exposure to UV radiation, a light sensitive material, called photoresist, experiences a change in its solubility properties. By the selective exposure and removal of the resist, the desired pattern can be defined on the substrate. The photoresist can be divided in two types, namely positive and negative. Radiation with UV light changes the resistance to the developer solution. In case of a positive resist the exposed regions become more soluble [46]. This causes the exposed material to be etched away by the developer. If the exposed resist becomes polymerized, like in case of a negative resist, it is more difficult to remove it from the surface and only the exposed regions remain after developing [47].

Prior to the photolithography, the substrate with the imprinted nanowires were heated up to a temperature of 130 °C for 2 minutes, in order to remove adsorbed species and water from the nanowire surface. This initial cleaning step ensures adhesion of the resist on top of the silicon

wafer. Deposition of the photoresist was done by spin coating. By spinning at high speed, a uniform layer was created on top of the entire surface with excess being thrown off. In our case, TI 35ES from the company MicroChemicals GmbH was used as photoresist. This type of material is considered to be a positive resist.

To ensure that the resist does not change its properties a softbake process was performed. A stabile film is obtained by removing the excess of solvent after spin coating. This step is important to make the resist sensitive for the following lithography. The respective processing steps are depicted in figure 10.

A mask, consisting of 15 pairs of electrodes, was aligned with the surface and selective areas of the resist were exposed with UV light. Subsequently, the substrates were kept at room temperature for 10 minutes, in order to diffuse out the hydrogen formed during the UV exposure. By heating the coated substrate up to 125 °C cross-links are formed, which make the exposed areas insoluble. This process is known as the reversal bake and results in a reversed image. The unexposed areas become soluble after flood exposure without the mask. By immersing the exposed substrate in a developer solution, the exposed regions will dissolve. The resulting pattern of contact structures on the silicon wafer is an exact copy of the mask.

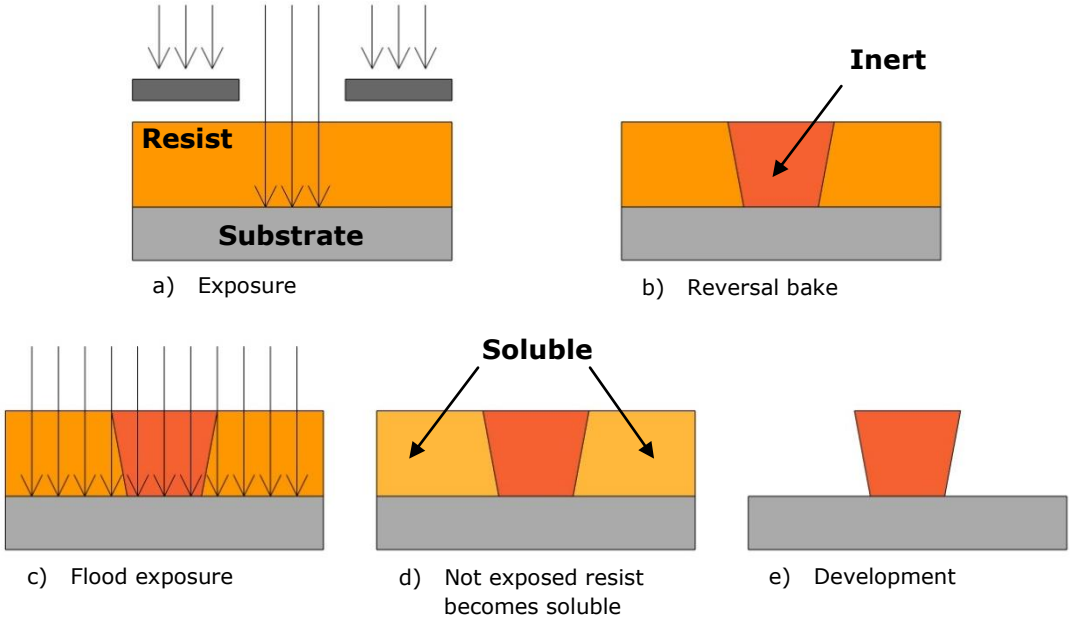

Figure 10: Processing steps of the photolithography process.
a) After alignment of the mask, the surface is exposed to UV light.
b) The reversal bake process activates the unexposed resist which makes it photosensitive
c) Flood exposure without mask.
d) The resist, which was covered by the mask, becomes soluble.
e) Immersion in a developer will dissolve the areas, which are not exposed to the light.

3.2.3 Metal deposition

The pre-patterned sample is processed to metal electrodes by means of electron beam evaporation. In this process, a metallic filament is heated up until it starts to emit electrons. These electrons are deflected toward the source material, which is located in a crucible under high vacuum. Hitting the target causes the kinetic energy of the electrons to be converted into heat. The target material is vaporized and deposited on a substrate opposing the crucible. This results in the deposition of a thin film on the substrate.

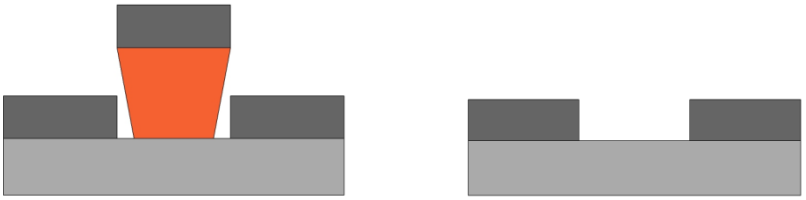

(a) (b)

Figure 11: Schematic illustration of predefined contacts.
a) Schematic representation of the substrate after metal deposition by electron beam evaporation.
b) Predefined contacts after lift-off of the remaining photoresist.

For the metal contacts on both sides of the ZnO nanowires titanium and gold, 10 nm and 150 nm respectively, were deposited onto the developed photolithography mask. Prior to gold evaporation, a layer of titanium is placed on top of the substrate in order to ensure a better adhesion between the SiO_2 on the substrate and the gold [48]. After lift-off of the remaining photoresist with aceton, only the predefined contact structures remained. The resulting contacts served as source and drain electrode. The gate is given by the conductive silicon substrate under the SiO_2 layer. A SEM image of a single nanowire between the two contacts is shown in figure 12. Finally, the substrates were glued with silver paste on a commercial chip suitable for the electrical measurements.

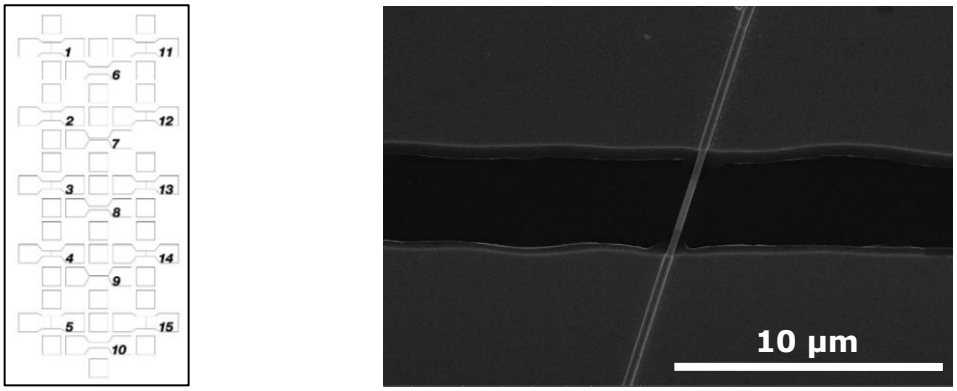

(a) (b)

Figure 12
a) Schematic representation of the mask used for photolithography process.
b) Representative SEM image of one contacted nanowire.

3.3 Characterization

3.3.1 Electrical characterization

Electrical measurements were performed in the probe station EP6 delivered by Süss MicroTec (Dresden, Germany), using the Source-Measure Unit (SMU) model 237 of Keithley Instruments (Cleveland, Ohio). The SMU was capable of simultaneously sourcing and measuring current and voltage at a set bias voltage with a sensitivity down to ~1 pA. For investigating the photoconductivity properties, the probe station is equipped with a light emitting diode (LED) with a central wavelength of 370 nm. By changing the external voltage difference applied to the LED, it was possible to vary the light intensity.

One of the simplest measurements is the I-V measurements. This includes the investigation of the current as function of the applied voltage. Different device properties can be obtained from the I-V characteristics, including output current, resistivity,… Also the quality of the contacts can be derived from these results [49]. In a second approach, the current flowing through the wire is measured as a function of the time. This is in particular interesting for the investigation of the presence of the persistent photoconductivity effect.

3.3.2 Scanning electron microscopy

In addition to the electrical characterization, the morphology of the nanowires was examined using SEM. SEM is a technique for high resolution imaging of structure sizes below the wavelength of visible light [50]. By scanning the sample with a focused beam of electrons various signals can be detected. These signals contain information about the sample composition, morphology, orientation, structure,… Signals comprise secondary electrons, backscattered electrons, x-rays, and electron beam current (EBIC). The image is built up by combining the obtained signal with the position of the beam. The morphology of the sample is obtained by collecting the signal from secondary electrons emitted from the sample surface. Images based on these secondary electrons display the topographic structure of the sample and where used to characterize the contacted nanowires in this thesis. The microscope used in the frame of this thesis was a Helios Nanolab 600i, delivered by FEI systems.

3.4 Ion implantation

Ion implantation is used for selectively implanting ions into a solid. This engineering process can be used for modifying the physical and electrical properties in a desired way. Ion beam implantation was performed using the implanter ROMEO, from the company High Voltage Engineering Europa, which allows implantation of nearly every element with ion energies from 20 keV to 400 keV and current densities up to tens of $\mu A/cm^{-2}$ [51]. The ions generated by the ion source are separated in a magnet by the Lorentz force. In this way ions of a particular mass with the desired charge state are selected. After passing through the selection magnet, the ions are accelerated to high

energy and directed to the target material. Finally, the sample is homogeneously scanned according to a Lissajous figure in order to receive a homogeneous lateral irradiation.

Before each implantation the relevant parameters were found using computer simulations. The ion energy needed to achieve the desired penetration depth was calculated using Stopping and Range of Ions in Matter (SRIM) [52]. SRIM is based on a Monte Carlo algorithm. Calculations of binary collision between the introduced ions and the target atoms provide an estimation of the ion distribution in the target material. Because of the use of flat surface geometries this program is limited to laterally homogeneous samples [53].

Two different ions are used in the described experiments: argon and aluminum. Since argon belongs to the noble gasses, irradiation with argon introduces only defects and no direct doping in the ZnO crystal. The noble gas is used in order to eliminate chemical effects in the nanowire [54]. On the other hand, aluminum is an n-type donor in ZnO. The introduced dopants will contribute to the increase of the electron density and influence the conductivity in addition to introducing defects. By comparing the results from argon and aluminum irradiation the effect of defects and doping can be separated. Typical implantation parameters for this thesis are summarized in table 1 together with the calculated ion ranges and straggling.

To get rid of the damage introduced by the implantation, a subsequent annealing was performed at 300 °C. The annealing time was progressively increased from 30 min to 8 hours. In this way defects are annealed and the implanted dopants may be activated.

Table 1: Overview of the implantation parameters for Argon and Aluminum.

	Argon	**Aluminum**
Ion Energy	160 keV	100 keV
Ion Fluence	$1{,}11 \times 10^{14}/cm^2$	$1{,}25 \times 10^{14}/cm^2$
Beam current	80 – 120 nA	120 nA
Ion range [SRIM]	100,7 nm	98,9 nm
Straggling	40,1 nm	43,6 nm

3.5 Photoluminescence

The photoluminescence (PL) process is characterized by the emission of light radiation from a material after absorption of photons. The energy released in the recombination of the created electron-hole pairs is emitted as a photon with respective wavelength. PL measurements are nondestructive and straightforward, which makes them an easy tool for studying fundamental optical properties, including exciton-phonon emission and band gap emission [55]. PL measurements were performed in order to characterize the optical properties of the contacted and implanted nanowires, as well as their defect levels in the band gap. The samples were placed in a liquid-helium cryostat at 4 K, in order to minimize temperature-induced broadening of the emission bands. A He-Cd laser with a wavelength of 325 nm was used as excitation source. Spectra were typically integrated for Y seconds.

4 Results and Discussion

4.1 Properties of undoped ZnO nanowires

Undoped ZnO is considered as an n-type semiconductor because of intrinsic defects such as zinc interstitials [56]. These defect states may influence the photoconductivity and photoluminescence of ZnO nanowires. This chapter reports about the fundamental processes and the role of surface effects on the electrical properties and the UV photoconductivity.

4.1.1 Electrical properties

The electrical characterization of ZnO NW FETs was performed before and after modification, in order to study the effect of defect engineering by ion implantation. In a first approach, the current through the nanowires was measured as a function of the applied voltage in the so called I-V characterization. This was performed at room temperature in ambient air by contacting the Ti/Au electrodes via two micromanipulators. The output curves of two typical devices prepared without any treatment are shown in figure 13. The curves are measured at voltages varying from -10 to +10 V.

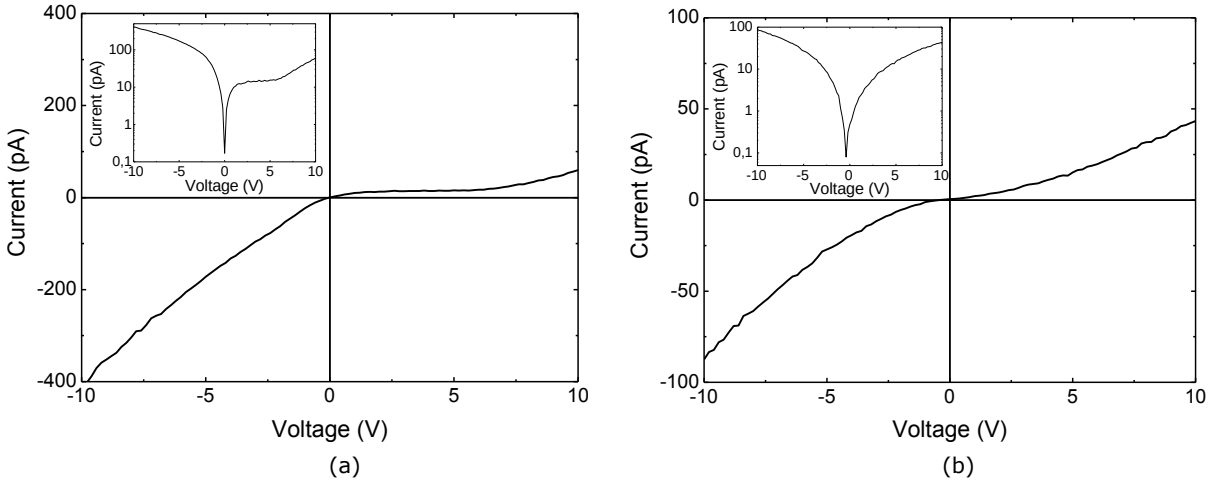

Figure 13: I-V characteristics of contacted ZnO nanowires.
The output curves of a typical ZnO nanowire FET are characterized by Schottky contacts. The inset shows a logarithmic representation of the linear plot.
a) I-V curves of the single nanowire device are typically asymmetric.
b) Multiple nanowire FETs show a more symmetric behavior since the characteristics of individual nanowires are averaged out.

It can be seen that the I-V curves of as-grown nanowires exhibit non-linearity. As one can see in figure 13 (a), the current is linearly proportional to the applied voltage in the negative voltage range. However, the slope of the curve is flat between 1 and 6 V, after which the current rises again. These output characteristics can be attributed to the formation of a Schottky barrier between the nanowire and the Ti/Au electrodes. In case of n-type semiconductors, this barrier originates at the semiconductor-metal interface when the difference between the work function of

the metal ϕ_m and the electron affinity of the semiconductor χ_{SC} is higher than zero. It is inconclusive whether the Schottky barrier observed in figure 13a is due to the model described by Schottky and Mott, since literature reports a work function of ZnO between 3,7 and 4,5 eV [57,58]. This suggest that it can be higher or lower than the titanium work function of 4,33 eV [59].

It is however likely that the titanium in the ZnO – Ti/Au contact is oxidized leading to a semiconductor–insulator–metal heterocontact. Such contacts can also have rectifying properties. The I-V characteristics typically observed in our samples therefore can be modeled by the formation of two Schottky barriers on both contacted sides of the nanowire. As observed in figure 13 (a), it is important to take a broad voltage range since the asymmetrical behavior is often only observed at voltages larger than a few volts.

Thus, a possible explanation for the asymmetric shape can be explained by considering the sample preparation. By imprinting the samples, the nanowires are randomly spread on top of the wafer, unaligned to the photolithography mask. This may cause that the length of the wire covered by the contact may differ on both sides resulting into different Schottky contact properties.

The applied imprinting procedure may also lead to both single nanowire (figure 13 (a)) and multiple nanowire devices (figure 13 (b)). In the last case the characteristics of different nanowires are measured in parallel. The rectifying and asymmetric contributions of the individual wires are average out resulting into a more linear and almost symmetric shape.

4.1.2 Thermal stability

Thermal stability refers to the stability of the ZnO nanowires at high temperature or in other words to the maximum temperature that can be applied before the nanowire starts to degrade. If ZnO nanowires are integrated into devices such as for gas sensors, they must be able to withstand high temperatures. Additionally, it is important to understand the impact of temperature on the nanowire properties, since fabrication processes as dopant activation and repair of the crystal structure after ion implantation involve high temperature annealing [60].

The impact of annealing to as-grown ZnO nanowires was evaluated by performing an electrical characterization before and after annealing. The complete devices including the contacts were annealed at 300 °C for 30 minutes and measured at the probe station. The same device was then annealed for 4 hours and measured again. This process was performed with progressively increasing annealing time from 30 minutes to 8 hours. The obtained results are depicted on both a linear and logarithmic scale as shown in figure 14. The black curve corresponds to the measurements performed before annealing. The green and blue curves, corresponding to respectively 4 and 8 hours annealing coincide in case of the linear graph (figure 14 (a)). A decrease in current is visible as the annealing time increases. An explanation involves the surface states. Adsorption of oxygen during the annealing lead to increased surface band bending [61], which determines higher resistivity of the nanowire. The logarithmic plot in figure 14 (b) shows an

asymmetric profile, characteristic for Schottky contacts. The non-zero current at 0 V bias is an indication that a response of the measurement setup is measured and not the current flowing between drain and source. This shows the extremely high resistivity of the sample after the corresponding annealing procedures. After such an annealing procedure, the degradation of the FET devices could be a result of an increase in defect density leading to disturbance of the crystallinity [62]. However, this is unlikely as the material ZnO itself is stable to temperatures up to 700 °C [63], which were not reached in these experiments. Further and more likely explanations are strong modification of the contact properties due to alloying at those temperatures, or changes in the surface morphology [64].

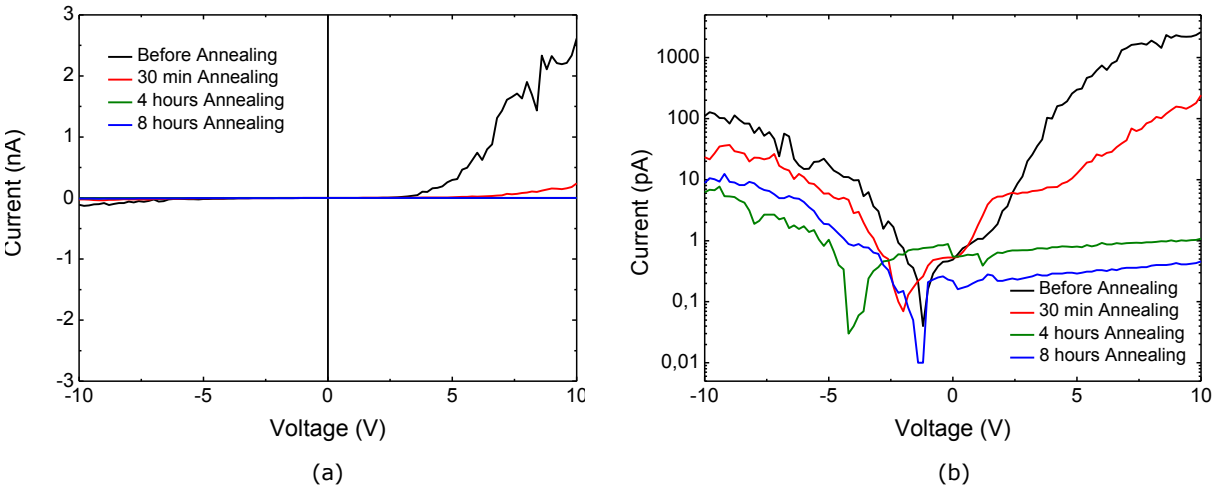

Figure 14: Electrical properties of as-grown ZnO nanowires after different annealing conditions.
The comparison of I-V curves obtained before and after annealing at 300 °C, plotted on a linear (a) and logarithmic (b) scale. The plots are characterized by an asymmetric profile attributed to the presence of Schottky contacts. Increase of the annealing time results in a progressive decrease in the current.

4.1.3 Photoconductivity

The photoconductivity for ZnO nanowires was studied under different light intensities with two distinct goals, namely the investigation of the increase of the photocurrent and the investigation of the dynamics of the photocurrent decay. ZnO nanowire FET devices were exposed to UV light of a light emitting diode whose light intensity was varied by changing the applied external power. The increase of the photoconductivity was investigated under high excitation (5 mW) and low excitation (20 µW) conditions. The measurements are shown in figure 15.

After stabilization of the current for 60 seconds the LED was switched on, generating electron-hole pairs. Migration of the photogenerated holes toward the surface lowers the probability of carrier recombination. The resulting increase in electron lifetime leads to an initially fast increase in photoconductivity. As the holes recombine with the trapped electrons, oxygen is desorbed from the surface of the nanowire. This induces a reduction of the trapped electrons as well as the height of the band bending. The drop ensures that the electrons can reach the surface more easily favoring oxygen re-adsorption. This leads to slowing down of the current increase and eventually the

electrical properties achieve a steady state when the oxygen absorption and desorption rate reach an equilibrium. Subsequently, the UV light was switched off and returned back to the original dark current with a long decay time, which will be discussed below.

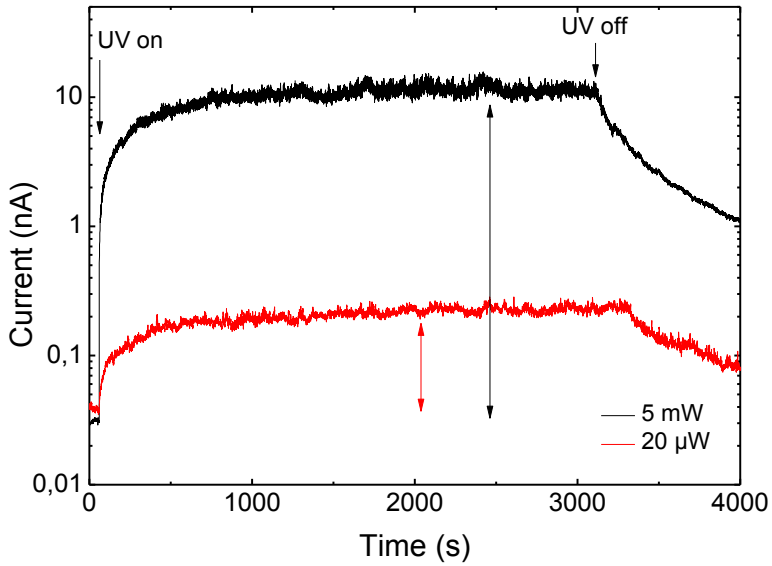

Figure 15: Photocurrent under steady state conditions.
Switching on the LED, after 60 seconds current stabilization, results initially in a fast increase, which slows down when oxygen absorption and desorption rate reach an equilibrium, leading to saturation of the photocurrent.

Measurements of the photocurrent of ZnO nanowires after different annealing procedures are compared in figure 16. The photocurrent is proportional to the concentration of photogenerated charge carriers and can be determined by subtracting the dark current from the current under illumination under steady state conditions. The results for low excitation power are depicted in figure 16 (a). The as-grown sample, characterized before the annealing procedure, shows a photocurrent of 80 pA. As the annealing time increases, there is a decreases in the photocurrent to 0,84 pA after four hours annealing. Annealing for a longer time leads to a slight increase to 4,5 pA. In comparison, the results for a high illumination intensity of 5 mW exhibit a similar profile (figure 16 (b)). The photocurrent decreases from 400 pA before annealing to 40 pA after four hours annealing. Eight hours annealing gives rise to an increase in the photocurrent to 82 pA. Therefore, both illumination intensities show the same behavior.

The deterioration of the photocurrent can be attributed to the thermal behavior of the contacts. At such temperature, the annealing process adversely affects the contacts, leading to slight instability and degradation of the device performance.

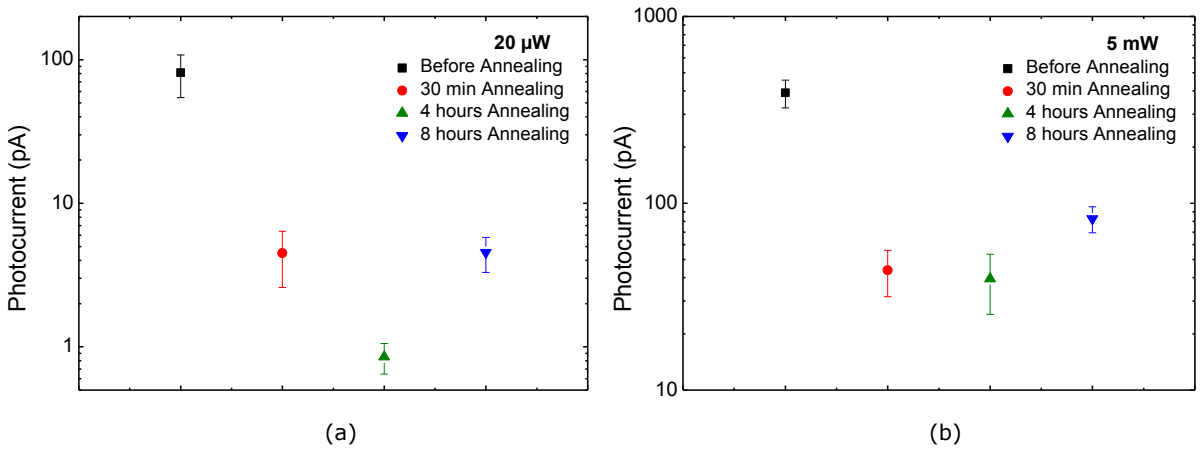

Figure 16: Photoconductivity of ZnO nanowires under different illumination intensities.
For both illumination intensities, low (a) and high (b), the device shows a decrease of the photocurrent and reaches the lowest value after four hours annealing. Only after eight hours annealing, a slight increase was observed, however the photocurrent is still lower compared with before the annealing process.

4.1.4 Dynamics of photocurrent decay

The dynamics of the photocurrent decay after UV excitation is investigated by considering the recovery time as a function of the excitation power. Here, the recovery time is defined as the time required to observe the complete decay of the photocurrent. Higher UV intensities result in faster trapping of electrons on the surface leading to a slower recombination and a larger recovery time. The photocurrent decay of ZnO nanowires as a function of time and excitation power is shown in figure 17. Each measurement starts with a stabilization period of 60 seconds, followed by UV excitation of 5 seconds. Subsequently, the UV light is switched off. While keeping the bias voltage set at 1 V, the UV excitation power is progressively increased.

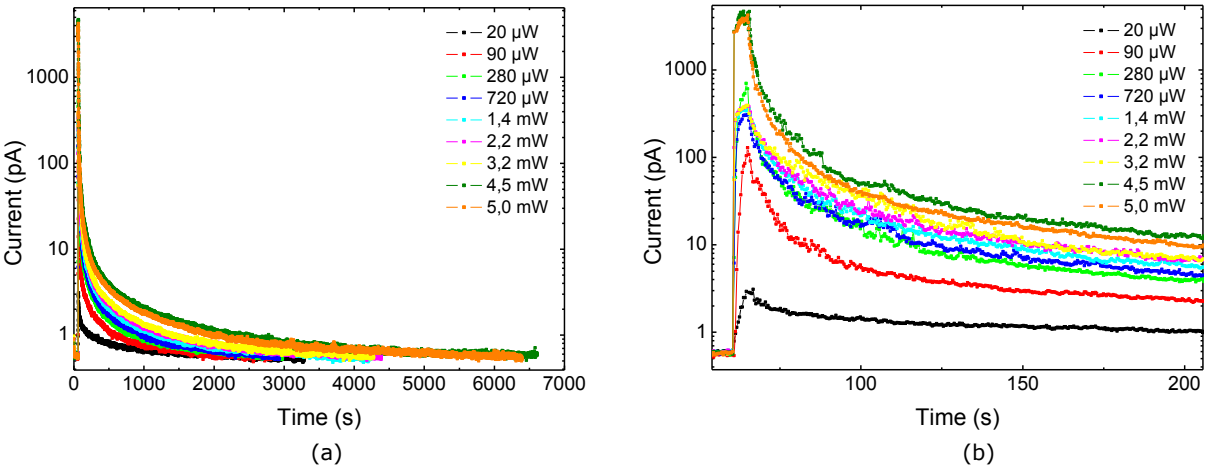

Figure 17: Dynamics of the photoconductivity decay.
Full (a) and enlarged (b) plot of the current through one ZnO nanowire after exposure to UV light. After switching of the UV light, oxygen at the surface traps electrons from the conduction band, leading to a higher surface barrier. The band bending slows down the recombination of electron-hole pairs due to spatial separation of electrons and photogenerated holes. This process is highly influenced by surface effects.

Upon exposure with UV light, the photocurrent increases instantaneously. By varying the exposure intensity from 20 µW to 5 mW, the current increases from one to four orders of magnitude. A magnification of the full curve (figure 17 (a)) is shown in figure 17 (b), in order to illustrate the photoresponse in more detail. It can be seen that the current increase consists of a fast component in the first seconds of excitation and afterwards a slow component takes over. After turning off the UV light, the initial decay of the current is fast but proceeds progressively more slowly. Eventually, it took more than 6000 seconds to restore the current to its original level.

The fast photocurrent component is attributed to a bulk process in which electron-hole pairs are generated [65]. Subsequently, a slow surface-related process further increases the conductivity via oxygen adsorption and desorption. After trapping of photogenerated holes at the surface, the unpaired electrons can contribute to the conductivity [10]. By increasing the illumination intensity, more carriers are generated. This in turn leads to a higher photocurrent.

The decay time is also strongly influenced by surface effects due to the high surface-to-volume ratio of nanostructures. When the UV-light is turned off, electrons from the conduction band are trapped by adsorbed oxygen molecules resulting in photocurrent decay. As a result of the trapping, the surface bands start to bend and give rise to a higher internal electric field. The increased barrier reduces the amount of oxygen adsorption leading to a spatial separation of electrons and photo-induced holes. This separation hinders the recombination of electron-hole pairs resulting in a higher recombination lifetime. Therefore, the decay of photocurrent and the presence of a long tail are strongly related to the surface band bending.

To get a better understanding of the photoconductivity decay, the recovery time was plotted in figure 18 as a function of the excitation power, in the range 20 µW to 5 mW. The two Y-axes are independent of each other and correspond to a recovery time of respectively 75 % and 100 %. The full recovery time increases as the excitation power increases. However, the time required to observe only 75% of the photocurrent decay shows an opposite dependence.

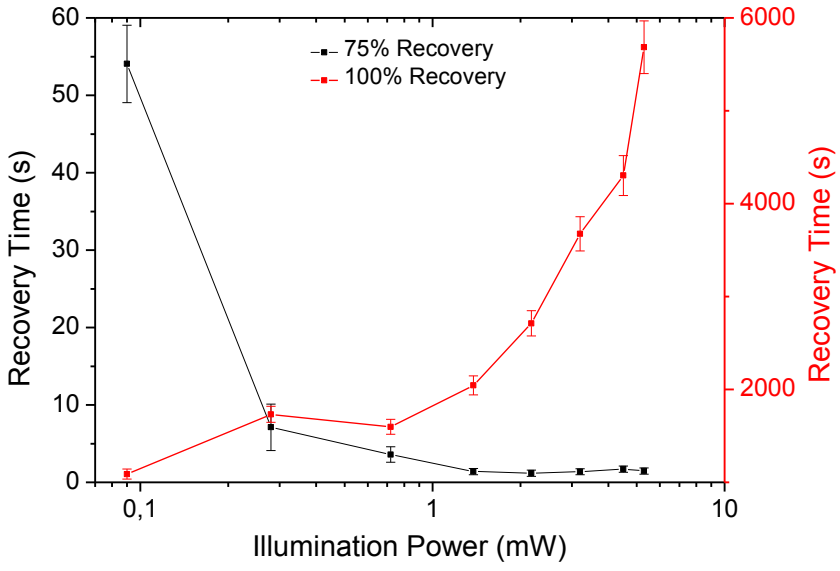

Figure 18: Variation of photocurrent with UV light intensity.
Excitation with low intensity creates only a few electrons, resulting in a small decrease of the band bending. Because of this the recovery time is high for the 75 %. However, illumination with higher intensities leads to a decrease in the band bending, leading to a decrease of the recovery time. Reaching 100 % recovery requires a long time since the increase in the number of trapped electrons, gives rise to an increased surface band bending.

This result can be interpreted as the migration of holes toward the surface during UV excitation inducing the discharge of the surface through desorption of negatively charged oxygen ions. As such, the illumination process causes a reduction of the surface band bending and it is reasonable to assume that higher excitation power will result in larger reduction of the surface band bending. Therefore, the trapping at the surface of photogenerated electrons immediately after illumination will proceed faster in case of higher excitation power, because electrons encounter a lower energy barrier. This explains why the partial recovery time (recovery time 75%) decreases as the excitation power increases. However, as long as the photocurrent decay process continues, the surface band bending rises progressively, lowering the rate of further electron trapping at the surface. Because there are more states at the surface for higher excitation intensities, the complete recovery time (recovery time 100%) nevertheless increases as the density of photogenerated electrons increases.

4.2 Properties of argon irradiated nanowires

Argon ion implantation can be used to tune the electrical properties of ZnO nanowires by introducing defects. Some of these disorders can be recovered using post-annealing procedures. Since argon is a noble gas, it does not induce chemical reactions or doping and cannot substitute lattice atoms. Therefore, electrical and photoconductivity measurements on argon implanted nanowires can be used as a reference for the influence of the aluminum implantation on the photoconductivity properties on ZnO nanowires.

4.2.1 SRIM simulation

The expected path of ions in the target was simulated using SRIM [52,53] in order to determine the range of the incorporated argon atoms in the target material. Taking into account the diameter of the nanowires, the ion range is determined by adjusting the ion energy, ensuring that the ions stop in the nanowire. An ion energy of 160 keV leads to an implantation depth of approximately 100 nm. The desired concentration of the order 10^{19} cm^{-3} corresponds to a fluence of $1{,}11 \times 10^{14}/cm^2$. Figure 19 displays the argon implantation profile for an implantation energy of 160 keV. The concentration of implanted ions as a function of depth is illustrated in figure 19 (a), and the corresponding ion trajectories in the target are shown in figure 19 (b) showing the lateral straggling.

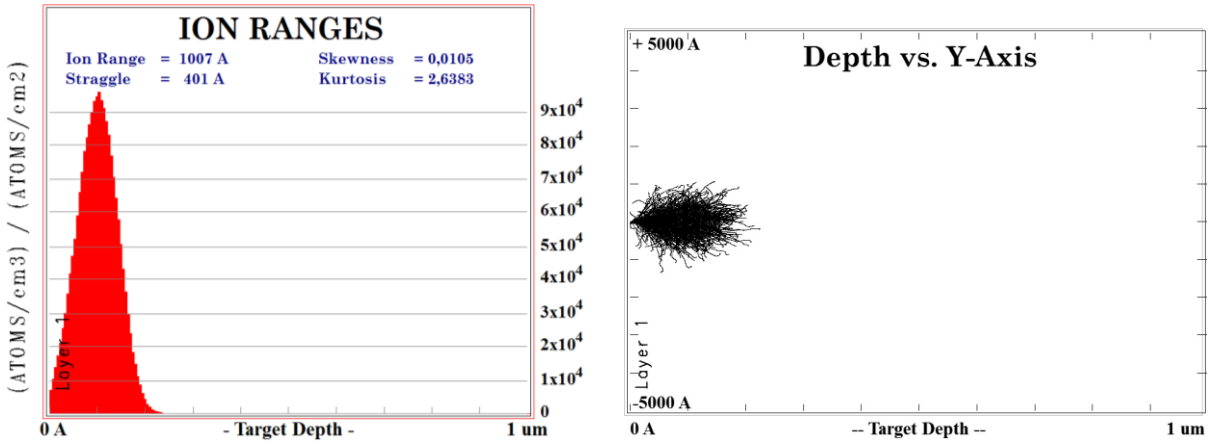

Figure 19: SRIM simulation results for argon implantation into ZnO nanowires.
a) Concentration of ions as a function of the depth. An implantation energy of 160 keV gives rise to an ion range of 100 nm.
b) Trajectories of implanted ions in ZnO bulk.

4.2.2 Structural properties

In order to determine if the implantation has affected the morphology of the ZnO nanowires, SEM analysis was performed before and after the implantation process. The occurrence of damage is related to the ion species, energy, fluence and the target material [66]. Typical SEM images are

shown in figure 20, before and after ion implantation. The image shows that irradiation with 160 keV and a fluence of $1{,}11\times10^{14}/cm^2$ does not introduce significant changes in the morphology of the surface and device. The implantation process does not introduce roughness; however, the decrease in wire diameter can be attributed to the prolonged measurements which are repeated several times.

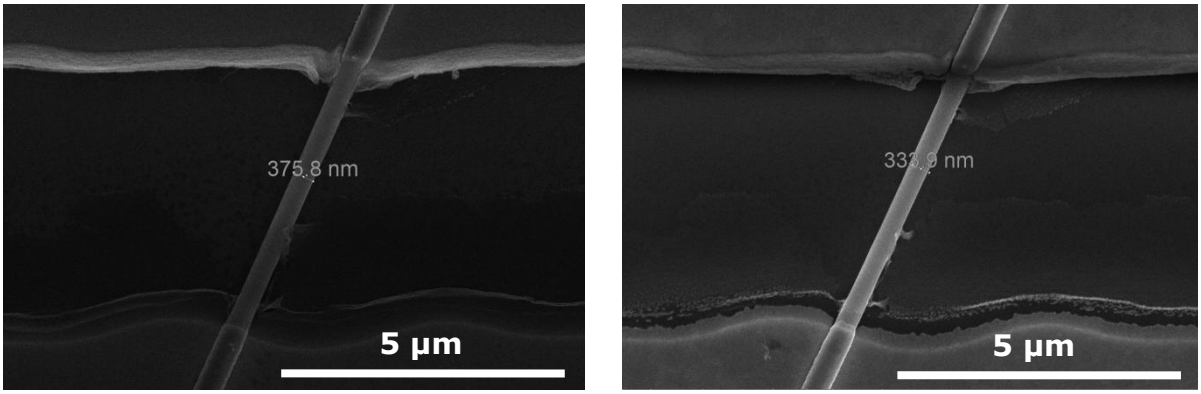

Figure 20: SEM characterization of ZnO nanowires.
SEM characterization of ZnO nanowires grown on silicon substrates before (left) and after (right) argon implantation. No noticeable change in structure and morphology is visible after irradiation with argon ions.

4.2.3 Electrical properties after thermal treatment

The electrical characteristics of the contacted nanowires in dark conditions were compared before and after argon implantation via I-V measurements. A summary of the electric properties after further different annealing conditions is shown in figure 21 for the exact same devices before and after ion implantation. The current was measured as a function of the applied voltage which varied from -10 V to +10 V. The black curve corresponds to I-V characteristics obtained before argon implantation. It can be seen that as-grown nanowires exhibited s-shape characteristics. The almost symmetric behavior implies Schottky contacts with similar properties on both ends of the nanowire, while the low current level shows that this is a highly resistive device.

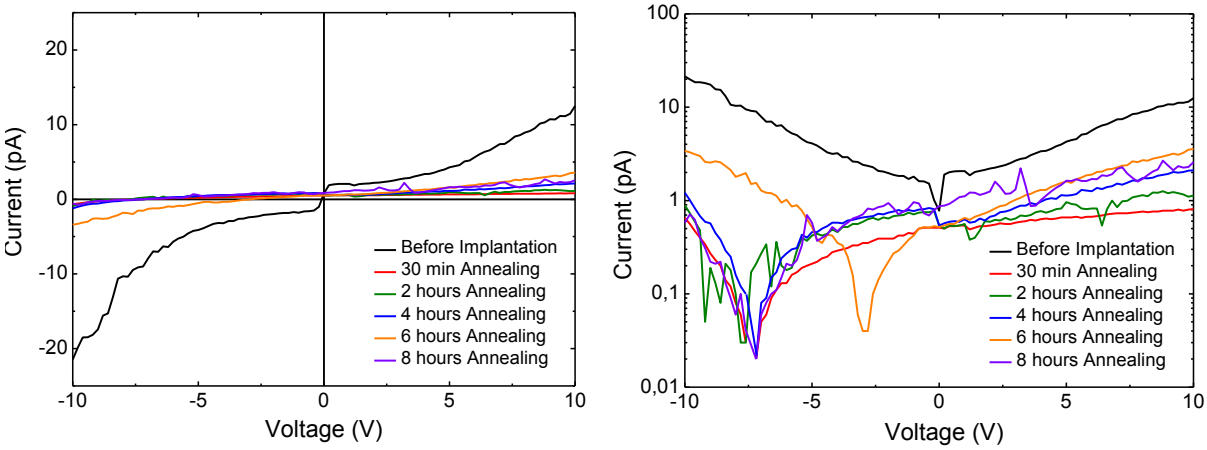

Figure 21: I-V characteristics of argon implanted ZnO nanowires after different annealing conditions.
Comparison of the I-V curves obtained after argon implantation with energy of 160 keV, plotted on a linear (left) and logarithmic (right) scale. The plots are characterized by an almost symmetric profile attributed to the presence of similar Schottky contacts on both sides. The wire shows a strong isolating character after implantation. Only six hours annealing leads to a little increase of the conductivity.

After 30 minutes annealing in air at 300 °C the implanted wires revealed almost no conductivity. This can be attributed to the large amount of defects still present in the crystal lattice. High temperature annealing causes diffusion of the defects out of the crystal, compensating for the created defects. However, the observed I-V curves suggest that the annealing was not particularly effective. Increase of the conductivity can be obtained by increasing the annealing temperature or the time. We decided to anneal the samples for a longer time, since this annealing temperature represents the optimized value, according to previous study [67], which showed that the contacts fully degrade at higher temperature. This is confirmed by the measurements of the thermal stability, as described in the previous section 4.1.2. So we performed an annealing at 300 °C and progressively increased the time from 30 minutes to 8 hours. Comparison of the observed curves indicates a strong isolating character after implantation. The absence of conductivity is likely related to defects that are still present in the crystal even after 8 hours annealing. A full recovery of the ZnO lattice structure after ion implantations requires temperatures well above 700 °C [68]. Another explanation may involve additional surface states, which have been introduced by sputtering of the surface leading also to increased surface band bending [61], which determines higher resistivity of the nanowire.

Another striking appearance is a voltage shift from 0 V to -7 V. Only 6 hours annealing gave rise to a small shift in the opposite direction. However, annealing longer than 6 hours led to a further degradation. Such a shift could be due either to the measurement of the internal resistance of the SMU, or to capacitance effects due to eventual charge accumulation at the interface between the electrodes and the nanowire. Since we observed a small photoresponse (see section 4.2.4), we suggest that the latter effect can be predominant, as no photoresponse would be observed in case of an electrode pair without nanowire in between.

4.2.4 Photoconductivity

Photocurrent measurements performed on argon implanted FET devices reveal almost no photoresponse. This is not surprising, as the nanowires became highly resistive after the irradiation and annealing did not recover their conductivity. Typical values of the photocurrent under different annealing conditions are presented in figure 22. Upon UV excitation with 20 µW no photoresponse has been detected after implantation with argon ions. Photoresponse was observed only after annealing for eight hours, but the current was almost one order of magnitude lower in comparison with the photocurrent value before implantation. Exposure of the device to higher intensities (5 mW) showed a decrease in photocurrent from 12,4 nA to 0,67 pA for four hours annealing. Annealing for longer time leads to a further decrease in photocurrent to 0,3 pA. A very small recovery in photocurrent is observed after eight hours resulting in a value of 2,0 pA.

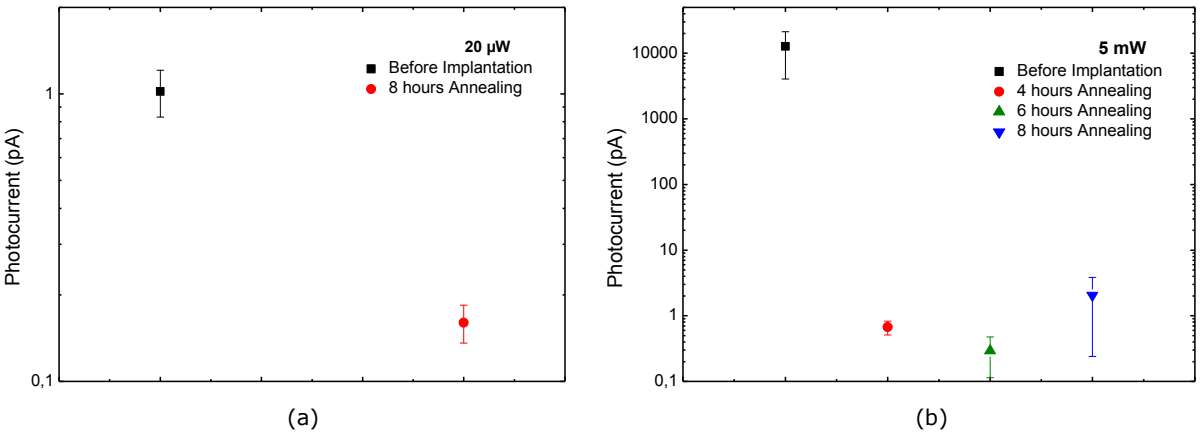

Figure 22: Photoconductivity of aluminum implanted ZnO nanowires under different illumination intensities.
(a) The FET devices show almost no response upon UV excitation. Only after eight hours annealing, a little photoreaction was observed for the lowest intensity of 20 µW, although much lower than before implantation.
(b) A decrease of several orders of magnitude takes place after illumination with 5 mW. After eight hours annealing a little improvement was observed, however the photocurrent is still lower compared with before the implantation process.

The previously described isolating character after implantation may contribute to the absence of a photoresponse. This testifies also of a low concentration of intrinsic electrons and the presence of oxygen vacancies and other defects in the wire. The progressive decrease in photocurrent upon higher illumination intensities may suggest that we exceeded the maximum annealing time and damaged the contacts. However, further increasing the annealing time revealed a not significant increase of the photocurrent. This suggests that the induced defects are still present in the crystal and need a longer time to diffuse out completely.

4.2.5 Dynamics of photocurrent decay

The photocurrent decay after UV excitation was studied as a function of three different excitation powers (20 µW, 1,40 mW and 5 mW). The comparison of the recovery time before and after argon implantation as a function of the induced photocurrent is shown in figure 23. By varying the light intensity from 20 µW to 5 mW, the photocurrent of the unimplanted sample rises with four orders of magnitude. A summary of the excitation power and the corresponding photocurrent, before and after UV excitation is represented in table 2.

The recovery times before implantation are 574 s, 2043 s and 5680 s for 20 µW, 1,40 mW and 5 mW (figure 23, black curve). After implantation, the same values of the excitation power are related to recovery times of 112 s, 295 s, 497 s (figure 23, red curve). A precise comparison of the recovery time is not possible, because the corresponding generated photocurrents differ considerably and in case of argon implantation are very close to the sensitivity of the SMU. Nevertheless the results suggest that the recovery time tends to slightly reduce after ion implantation.

The large recovery time before implantation can be ascribed to surface effects. After turning off the light, the increased band bending, due to trapping at the surface, forms a barrier for the electrons and holes to recombine. This spatial separation results in a longer lifetime and recovery time. This effect is more pronounced in the presence of high excitation intensities since higher excitation intensities result in easier trapping of electrons on the surface. In turn, this leads to a slower recombination and increase in the recovery time.

The reduction of the recovery time after argon implantation can be attributed to the generation of defects during implantation, which provide additional recombination paths for photogenerated electrons and holes and determines consequently a faster decay of the photocurrent.

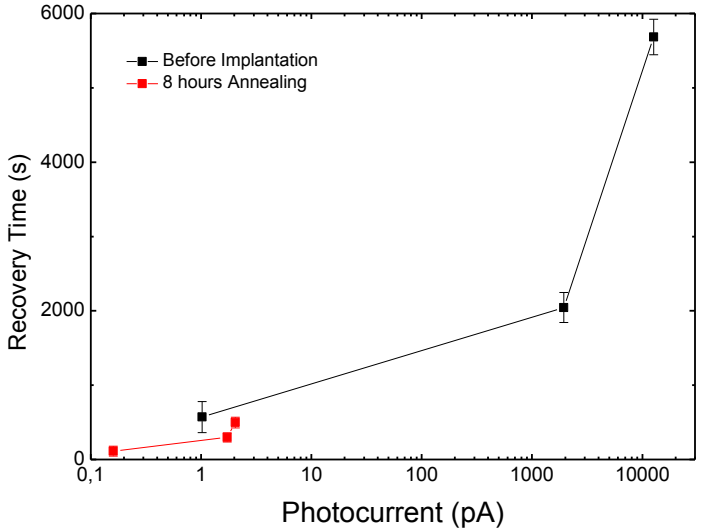

Figure 23: Dynamics of the photocurrent decay before and after argon implantation.
Comparison of the recovery time as a function of three different excitation powers. The photocurrent of the unimplanted nanowire increases several orders of magnitude. After thermal annealing, the photocurrent of the argon implanted sample increased only one order of magnitude. The difference in photocurrent makes it impossible to make a comparison of the obtained recovery time.

Table 2: Overview of the excitation power and the corresponding photocurrent before and after implantation.

Excitation power	Before implantation		After implantation	
	Photocurrent	Recovery Time	Photocurrent	Recovery Time
20 µW	1,03 pA	570,54 s ± 208	0,16 pA	112,36 s ± 65
1,4 mW	1,94 nA	2044,6 s ± 202	1,74 pA	296,80 s ± 60
5 mW	12,67 nA	5683,3 s ± 238	2,08 pA	497,36 s ± 72

4.3 Properties of aluminum irradiated nanowires

The electrical properties can be enhanced by introducing dopants. One of the main impurities in ZnO is aluminum because of its non-toxicity [69], low resistivity [70] and thermal stability [71]. It is known that aluminum can act as a shallow donor and improve the conductivity upon doping via ion implantation [72,73]. Within this chapter, the results of aluminum ion implantation in ZnO nanowires are presented.

4.3.1 SRIM simulation

As with the argon irradiation, the impact of introducing aluminum in ZnO nanowires was simulated. The ion range was again set to 100 nm to ensure that the dopants reach the core of the wire. Based on the collision of the aluminum ions and the target atoms an ion energy of 100 keV is needed to achieve the desired penetration depth. The ion fluence must be set to match the desired concentration. Fluences of $1{,}25\times10^{14}/cm^2$ lead to a concentration of 10^{19} m^{-3}. We obtained a similar implantation profile as compared to argon by adjusting the ion energy and the ion fluence. The estimated ion range and damage distribution are shown in figure 24.

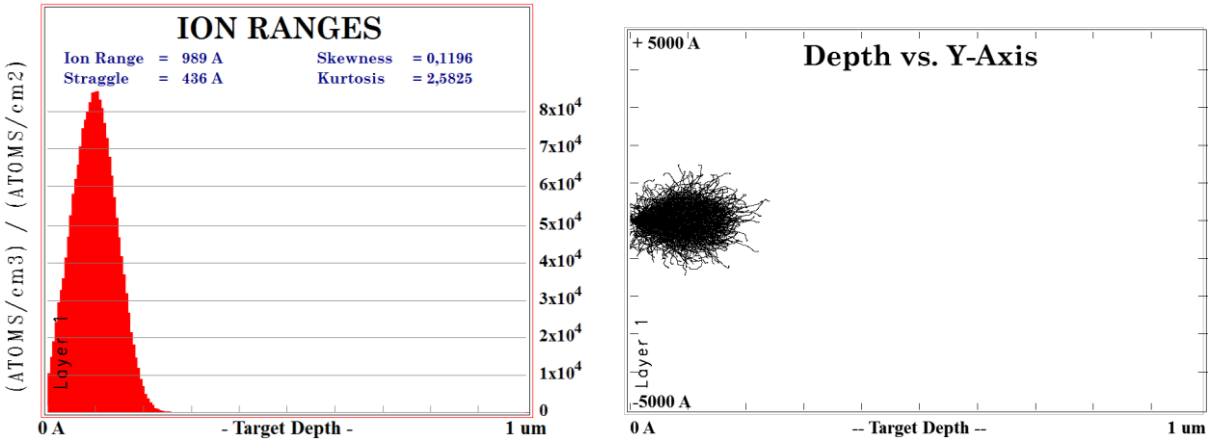

Figure 24: SRIM simulation results for aluminum implantation into ZnO nanowires.
a) Concentration of ions as a function of the depth. Implantation energy of 100 keV gives rise to an ion range of 100 nm.
b) Trajectories of implanted ions in ZnO nanowires.

4.3.2 Structural properties

SEM images taken from as-grown and aluminum implanted nanowires show no noticeable morphology changes such as holes or rough surfaces, such as for the argon irradiated wires shown in the previous section. As it can be also seen in figure 25, the diameter before and after implantation has the same value of around 420 nm. This suggests that the nanowire can resist both the ion irradiation as well as the repeated electrical measurements, which were taken before these SEM images and last for several hours. We are not able to say if the collisions during irradiation create defects like vacancies and interstitials at this magnification. However, Wesch et al. observed that ZnO does not amorphize at such low energy (100 keV) [74]. The nanowire retains

its crystallinity since most damage will be restored by dynamic annealing at the given irradiation temperature, but point defects will remain.

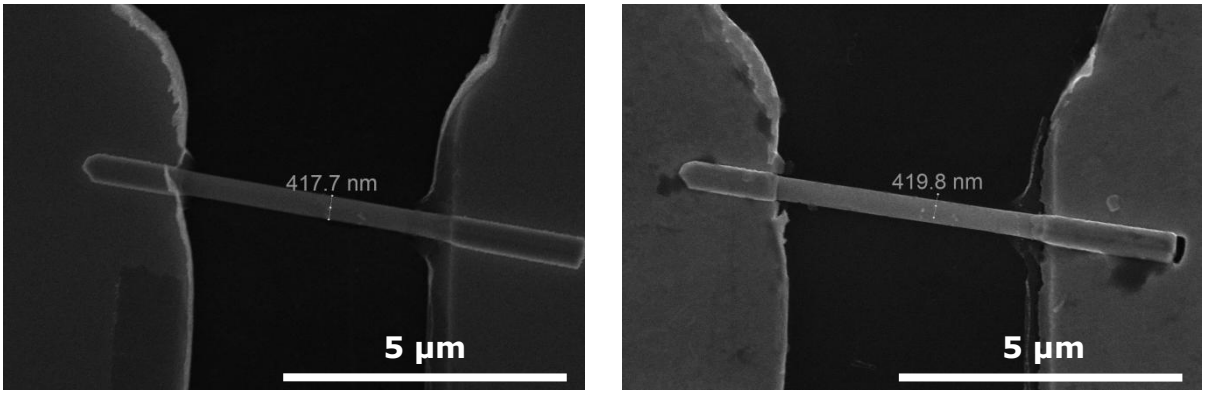

Figure 25: SEM characterization of ZnO nanowires.
SEM characterization of ZnO nanowires grown on silicon substrates before (a) and after (b) aluminum implantation and electrical measurements. Irradiation with 100 keV and $1{,}25\times10^{14}/cm^2$ does not introduce a significant change in morphology.

4.3.3 Electrical properties of as-implanted nanowires

Following aluminum implantation, the ZnO nanowire FET was quantitatively characterized using the probe station. The electrical conductivity, which is displayed in figure 26, was measured by sweeping the source-drain voltage and simultaneously measuring the current. The non-linearity can again be attributed to the Schottky barrier between the ZnO nanowire and the metal contacts.

The as-implanted wires show poor conductivity due to implantation associated defects introduced in the crystal structure, as also observed after the argon implantation. It is not a surprise that the implantation defects dominate the electrical properties. Even though dynamic annealing is effective in ZnO [74], each implanted atom still creates 10-100 point defects. In order to further remove the damage and activate the implanted impurities (here aluminum), one need to perform thermal treatments.

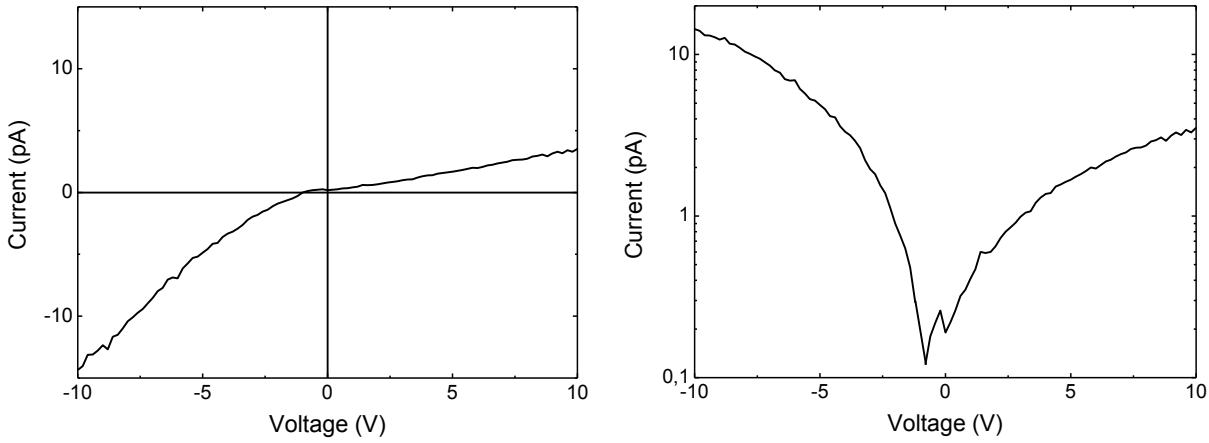

Figure 26: I-V characteristics of aluminum implanted ZnO nanowires before post-annealing.
Output curves of a typical ZnO nanowire FET are characterized by a non-linear behavior, typically for Schottky barriers. Linear (left) and logarithmic (right) representations of the I-V characteristics are obtained by varying the voltage from -10 V to + 10V. The implantation induced defects give rise to low conductivity.

4.3.4 Electrical properties after thermal treatment

In order to investigate the impact of n-type dopants on the electrical properties of ZnO nanowires, we have examined the electrical characteristics before and after the implantation process. Although the observed current is higher than the as-grown nanowire, the low conductivity of as-implanted wires suggests that subsequent annealing is essential. Introduced defects act as scattering centers and must be removed out of the crystal lattice. Because aluminum ions behave different than argon ions it is necessary to optimize the annealing procedure again. I-V characteristics of a representative ZnO nanowire are shown in figure 27 as a function of annealing time at 300 °C. Also in this case the non-linear behavior indicates that the contacts form a Schottky barrier.

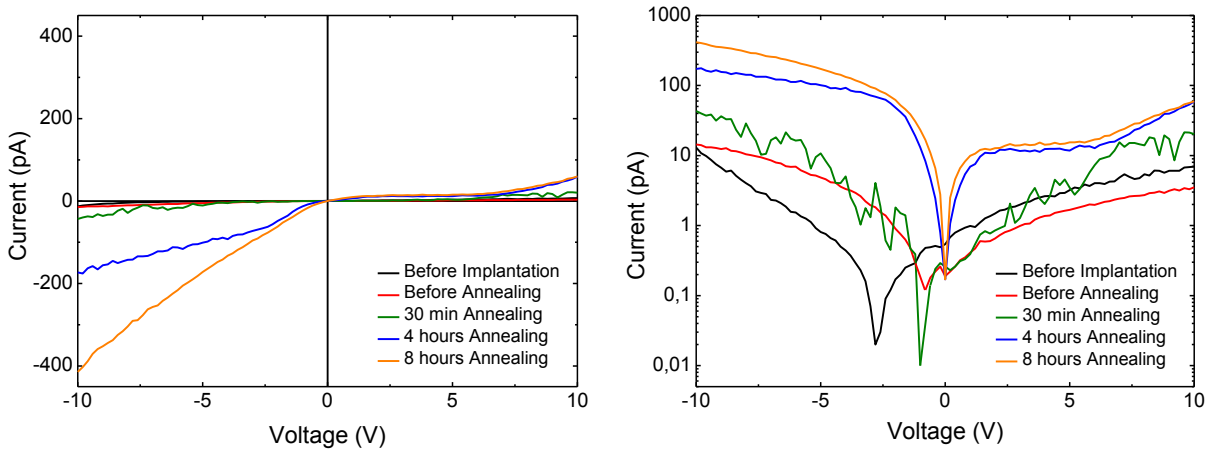

Figure 27: I-V characteristics of aluminum implanted ZnO nanowires after different annealing times at 300 °C.
Comparison of the I-V curves obtained after aluminum implantation with energy of 100 keV, plotted on a linear (a) and logarithmic (b) scale. The plots are characterized by an asymmetric profile attributed to the presence of a Schottky barrier. Annealing at 300 °C for four hours or longer leads to a significant increase of the conductivity.

After aluminum implantation, a small current was observed for the as-implanted sample since fewer defects are present in the crystal structure compared to the argon irradiation. This might be due to the fact that the implantation energy for aluminum (100 keV) was lower in comparison to argon (160 keV). However, the main reason is the presence of aluminum in the nanowire, which makes it more conductive due to its n-type dopant behavior in ZnO. Annealing for longer time results in a progressively increase of the current, as defects anneal out. The nanowire has the highest conductivity after annealing for 8 hours at 300 °C. The shift in voltage becomes zero after annealing for at least 4 hours.

Compared with the I-V curve of the unimplanted wire (black curve), the conductivity was increased by several orders of magnitude. Donor sites associated with oxygen vacancies and zinc interstitials give rise to electrons, which dominate the conductivity of unimplanted ZnO nanowires. During the implantation process, the aluminum ions undergo collisions and are stopped within the crystal. Most of these impurities stay at interstitial positions [66]. Annealing enhances the diffusion of the aluminum ions to substitutional sites and lead to an effective incorporation in the material. The

Al^{3+} ions incorporated on the substitutional sites of divalent zinc or in interstitial positions form shallow donor centers. This contributes to a higher free carrier concentration and gives rise to an increased conductivity. The effect observed after annealing indicates also that the implanted aluminum donors were not completely active immediately after irradiation.

4.3.5 Photoconductivity

The increase of the photocurrent was studied as a function of different annealing procedures. The photoconductivity of aluminum doped ZnO nanowires annealed for different periods is presented in figure 28. The graphs show that the as-implanted nanowire has the lowest photocurrent value of 3,50 pA, in agreement with the argon implanted samples. Annealing leads to an increase in the photocurrent by several orders of magnitude. After eight hours annealing the photocurrent under low excitation power reached the highest value of 3600 pA, as shown in figure 28 (a). In figure 28 (b), which shows the same device but under high illumination power, the highest photocurrent is observed after eight hours annealing (725 nA). Four hours has also a higher current in comparison with the untreated nanowire but is slightly lower. Further, the as-implanted wires exhibit the lowest value of 0,65 nA. Low and high intensity illumination reveal a similar profile, but the range of the photocurrent is different, respectively pA and nA.

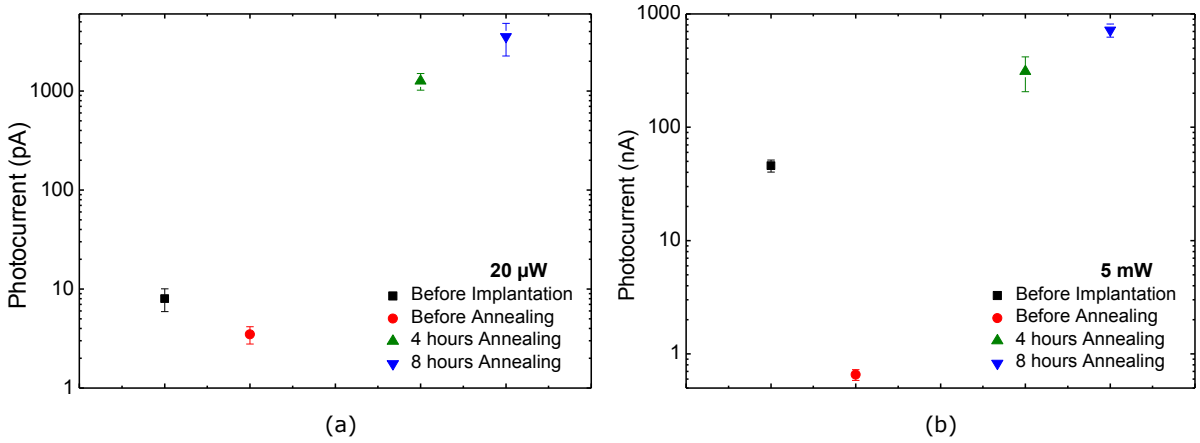

Figure 28: Photoconductivity of aluminum implanted ZnO nanowires under different illumination intensities.
For both illumination intensities, low (a) and high (b), the as-implanted nanowire shows the lowest photocurrent. Upon annealing, the photocurrent increases by several orders of magnitude which can be attributed to a higher number of free carriers.

Upon exposure to UV light, electron-hole pairs are created in the nanowires. However, the large number of defects in the as-implanted nanowire reduces their mobility. This stimulates recombination of the photogenerated electrons with the present defects and gives rise to a low concentration of electrons in the conduction band. However, annealing results in an activation of the aluminum dopants as well as to a reduction of the defects; thus, the better crystallinity of the aluminum doped ZnO nanowires show increased photoconductivity.

4.3.6 Dynamics of photocurrent decay

We performed electrical measurements before and after aluminum implantation, in order to investigate the change in the photocurrent dynamics. The recovery time as a function of varying excitation power after removal of UV light is shown in figure 29. The recovery of the implanted ZnO nanowire (red curve) to the initial level was much higher than that of the undoped device (black curve). We observed longer recovery times after implantation in the investigated photocurrent range. A summary of the excitation power and the corresponding photocurrent, before and after UV excitation is represented in table 3.

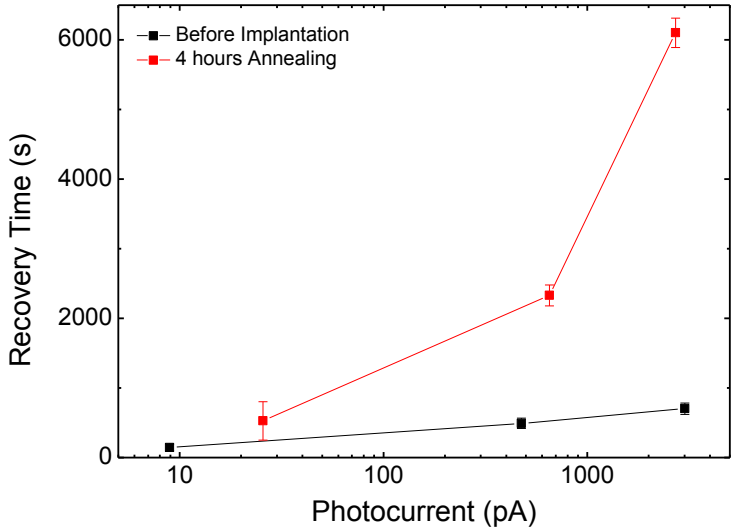

Figure 29: Dynamics of the photocurrent decay before and after aluminum implantation. Comparison of the recovery time as a function of three different excitation powers. The photocurrent of the undoped as well as the implanted nanowire increases several orders of magnitude. After thermal annealing, the recovery time increases significant due to trapping of electrons by additional surface defects. This results in a larger depletion region and consequently a more pronounced PPC.

Table 3: Overview of the excitation power and the corresponding photocurrent before and after implantation.

Excitation power	Before implantation		After implantation	
	Photocurrent	Recovery Time	Photocurrent	Recovery Time
20 µW	8,98 pA	145,16 s ± 50	25,68 pA	527,79 s ± 275
1,4 mW	475,94 pA	491,59 s ± 75	648,46 pA	2330,7 s ± 150
5 mW	3,04 nA	703,82 s ± 82	2,71 nA	6103,5 s ± 212

A discussion of the effect of the aluminum implantation process on the surface properties of the nanowires is required, in order to explain the obtained results. As mentioned in the introduction, the decay of the photocurrent is mainly determined by trapping of photogenerated electrons at the surface. The rate of this process depends on the width of the depletion region, which is given by [20]:

$$w = \sqrt{\frac{2\varphi}{N_d}},$$

where φ is the height of the surface potential barrier and N_d is the donor concentration.

Therefore, higher donor concentration should results in a smaller width of the depletion region, which should in conclusion lead to a faster rate of the electron trapping and reduced PPC. However, the implantation process might create additional surface defects (e.g. due to sputtering), which can act as trap for electrons in the dark. Creation of new surface states determines consequently an increase of the surface barrier φ, which is proportional to the concentration of electrons trapped at the surface. The latter process contributes to enlargement of the surface depletion region and to a more pronounced PPC. Therefore, aluminum doping of ZnO nanowires through ion implantation can have counteracting impacts on the PPC. If the density of surface defects generated by implantation dominates over the increase of the donor concentration, the depletion region of the aluminum implanted nanowires will be even larger than in the as-grown nanowires and the PPC will be more pronounced. Considering the experimental results, this seems to be the case of our nanowires. Additionally, the proposed model can explain the larger photoconductivity observed in case of doped nanowires. Indeed, as a result of the larger depletion region, photogenerated electrons and holes can be more effectively separated, according to the mechanism described in section 2.5. This determines a lower electron-hole recombination probability and consequently a larger photoresponse of the nanowires after aluminum implantation.

4.4 Optical properties

PL measurements were performed in order to get a better understanding of the correlation between implantation induced defects/dopants and the electrical properties on exact the same devices. The measurements were performed with a He-Cd laser. In order to avoid a strong increase of exciton-phonon interactions, which lead to broadening and overlapping of the PL bands, the samples were cooled down to a temperature of 4 K.

The optical properties are influenced by intrinsic as well as extrinsic effects [26]. The extrinsic effects are related to discrete electronic states in the bandgap, which are introduced by defects or dopants. The emission spectra of as-grown, argon and aluminum implanted nanowires are compared in figure 30. All measurements were conducted on single nanowires contacted by Ti/Au electrodes. Under laser excitation, the undoped ZnO nanowires exhibit two major peaks. One is the near-band-edge (NBE) emission with an energy around the bandgap of ZnO, related to the recombination of excitons. When an electron is excited to the conduction band, it still can be attracted to the corresponding hole in the valence band due to Coulomb interaction, giving rise to excitonic effects. The other emission band, located in the visible spectral range, is related to the recombination of electrons and holes at defect states in the band gap.

The deep level emission of undoped ZnO nanowires (figure 30, black curve), labeled DLE, is dominated by green luminescence at approximately 520 nm. This emission band originates from defects located at the surface as well as in the bulk. It is generally accepted that zinc interstitials and oxygen vacancies are the most common defects in undoped ZnO [75]. The most probable mechanism for the description of the green luminescence involves the recombination of a hole trapped in the single ionized oxygen vacancy and a delocalized electron near the conduction band [76,77]. The ionization state of the defects and therefore the properties of the DLE are affected by the formation of a depletion layer [76]. Due to the large surface-to-volume ratio, the emission intensity will increase when the width of the depletion region is reduced. This suggests that thin nanowires have a higher fraction of defect levels [78].

By normalizing the spectra to the NBE emission, as done in figure 30, it can be seen that the ratio between the NBE and the visible DLE emission decreases for the implanted wires. After implantation, we observed enhanced light emission originating from defects in the bandgap which are commonly located near the surface. The green luminescence at 550 nm can be attributed to the high level of defects in the crystal remaining after annealing. This suggests that the intensity corresponds to the higher amount of defect levels, which is in well agreement with the conclusions made out of the previous electrical measurements.

In comparison with the undoped sample, there is an additional contribution of a red emission band after argon and aluminum implantation. Based on electroluminescence spectra Alvi et al. concluded that more than one deep level defect is involved in this red luminescence [79]. Red emission appearing between 620 nm and 690 nm can be attributed to oxygen interstitials. This is caused by a transition from zinc interstitial to oxygen interstitial levels [80]. The luminescence in the range of

690 nm to 750 nm has a different origin. The emission ranging from 690 nm to 750 nm is linked to oxygen vacancies in ZnO [79]. Defect emission is also attributed to the presence of intrinsic defects introduced during the implantation and have not completely diffused out by annealing. So, the observed luminescence in the red band is a superposition of excess oxygen, zinc interstitials and surface dislocations [76]. In case of the aluminum implanted devices, the red emission band was even more pronounced. This can be attributed to recombination of Al^{3+} related donor centers with oxygen interstitials.

The additional band between 400 nm and 450 nm is due to an artifact of the PL setup, whereby the light is reflected back into the monochromator. Since the spectra are all obtained with a different exposure time, namely 0,1 s for the reference sample, 5 s for argon and 20 s for aluminum implanted devices, this band is the highest for the aluminum implanted nanowires (figure 30, red curve). A longer exposure time leads to a higher contribution of the artifact.

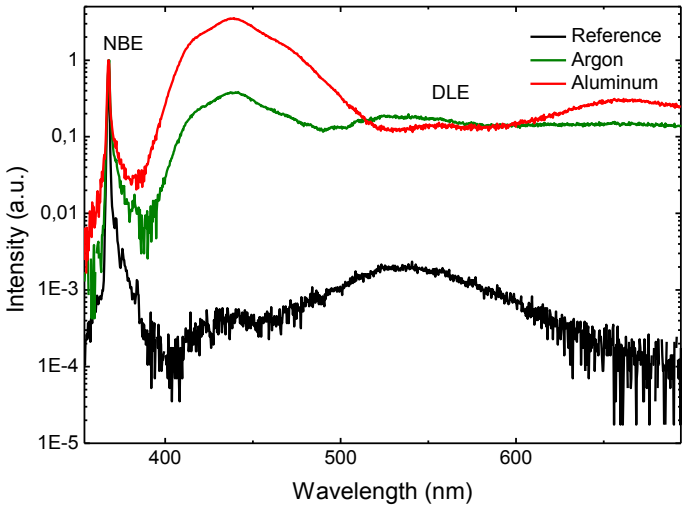

Figure 30: Overview PL spectra of ZnO nanowires.
The spectrum shows two emission peaks: the near band edge (NBE) and deep level emission (DLE). The DLE of the implanted samples is a superposition of green and red luminescence. The additional band ranging from 400 nm to 450 nm corresponds to a measurement artifact.

While the intensity of the DLE emission significantly increases, the NBE emission around 370 nm is reduced after implantation. A more resolved spectrum of the NBE emission is shown in more detail in figure 31. Several peaks can be observed, which correspond to the recombination of bound excitons. In the as-grown ZnO, the spectrum is dominated by a wavelength of 368,88 nm. This line, named I_6, corresponds to the recombination of excitons bound to aluminum [81]. This aluminum may be incorporated during growth from the boat used for the growth of the nanowires. Another explanation for the presence of aluminum can be attributed to intrinsic defects. On the high energy side, a peak shows up at a wavelength of 368,29 nm. The origin of this I_3* line is not specified, but it can be assigned to an ionized donor bound exciton transitions. However, it is also possible that the emission at this wavelength is related to a surface exciton (SX). Band bending ensures higher energies for SX relative to other bound excitons, but still lower than the energy of free excitons [61]. The presence of SX demonstrates contribution from surface states. However, in case of the SX one would expect a broader appearance of the peak. The right side of the prominent

I_6 line is characterized by I_{8a} and I_{10} at 368,35 nm and 369,87 nm respectively. However, in case of the SX one would expect a broader appearance of the peak. Apart from the donor bound exciton transitions, we observed two longitudinal optical (LO) phonon replica separated by an energy of 72 meV. The line labeled as I_6-1LO has a wavelength of 377,11 nm, which is at the position for the first phonon replica of the I_6. The second phonon replica, labeled I_6-2LO, is observed at 385,55 nm. The peak at 373,48 nm can be assigned to the two-electron satellite (TES) transitions of I_6.

In comparison to the as-grown nanowire, the NBE spectrum for argon exhibits a strong contribution of I_{8a} at a wavelength of 369,18 nm. Implanted argon ions can collide with zinc atoms in the crystal leading to a small change compared to the original position in the lattice. The obtained zinc interstitials can act as shallow donors. The donor bound excitation line I_4 at 369,72 nm is related to hydrogen. The highest energy shoulder observed at 367,31 nm is attributed to the free exciton, labeled as FX. According to Schilling et al. is the presence of FX correlated to high quality of the crystal surface [72]. However, the low PL emission after implantation and the strong isolating character of our devices indicate that a lot of defects are still present in the crystal after argon implantation. In addition, the features appearing around 377,10 nm and 385,55 nm can be assigned to the LO phonon replica of the zinc interstitials and are labeled I_{8a}-1LO and I_{8a}-2LO. The two phonon replica of the free exciton are located at 375,15 nm and 383,50 nm. Like the reference sample is the NBE emission of the aluminum implanted sample dominated by the line at wavelength 368,85 nm, labeled as I_5. The luminescence from this peak is correlated with the recombination of a bound exciton to an aluminum related impurity center. This confirms that the aluminum is incorporated in the wire. The TES, which is pronounced in the reference sample, disappears after implantation with argon and aluminum. Introduction of argon ions in the crystal leads to a reduction in the intensity of the phonon replica, which disappears completely after adding n-type dopants.

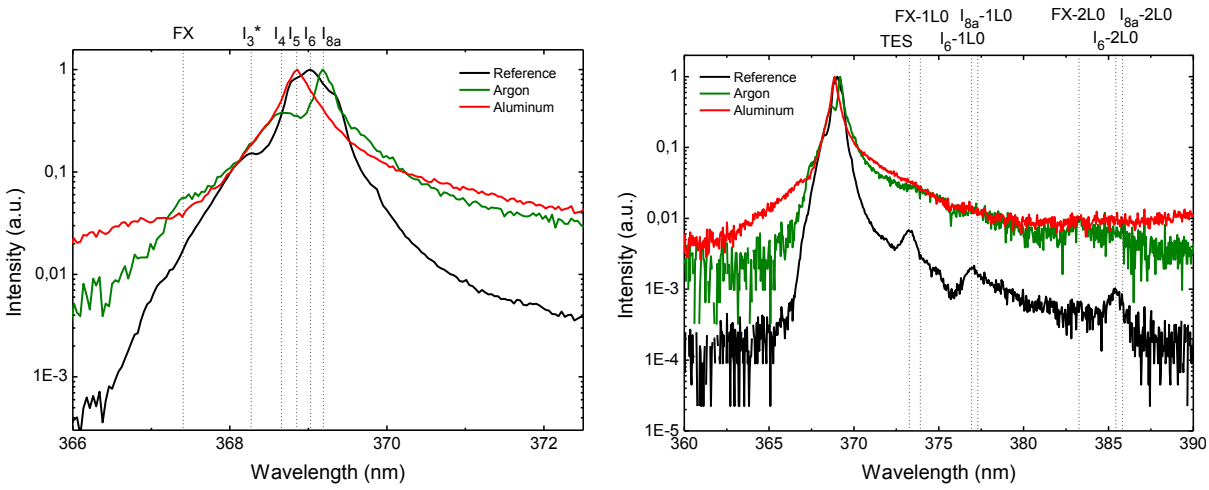

Figure 31: NBE PL spectra of ZnO nanowires.
The NBE spectrum of the reference sample is characterized by several donor bound exciton transitions, including aluminum (I_6) donor bound exciton. The origin of the lines I_3^*, I_{8a} and I_{10} are not specified. The peaks on the lower energy side correspond with the two-electron satellite and the first and second phonon replica of I_6. The green curve, corresponding to argon, is dominated by the I_{8a} line, the hydrogen related I_4 and the free exciton (FX). The peaks on the lower energy side correspond with the first and second phonon replica of the FX and I_{8a} line. Aluminum implantation (red curve) gives rise to the line I_5, which corresponds to the recombination of bound excitons with aluminum.

In conclusion, the optical experiments have shown that ion implantation causes a rearrangement in the crystal lattice. Both argon and aluminum bring about a reduction in the UV/visible intensity ratio with increase of the DLE and a decrease of the NBE transitions, due to the defects, which are still remaining even after the 300 °C annealing procedure. However, the clear presence of the I_5 line after aluminum implantation, confirms that the aluminum ions are properly incorporated in the crystal on substitutional sites. In addition, the LO phonon replica and TES transitions, which are pronounced in the undoped nanowires, diminish after argon irradiation and eventually disappear completely after the introduction of aluminum. This is clear evidence that the emission of ZnO nanowires is influenced by implantation.

5 Summary and Outlook

Among semiconductor nanostructures, ZnO nanowires have attracted a lot of attention because of their physical properties, such as a wide direct band gap and high conductivity. Because of this ZnO nanowires can function as building blocks for academic research and industrial applications. The UV photoresponse under diverse environments renders ZnO suitable in areas of sensors, photonics and electronics, including photodetectors, environmental control and optical switches. Selective modification of the surface properties through doping procedures makes it possible to fine-tune the material to favored properties.

The ZnO nanowires used in this thesis were synthesized using the so-called VLS growth method. The grown nanowires were assembled in a FET geometry in order to conduct electrical measurement. Contacts have been defined to both sides of the wire via UV photolithography. After lift-off only the predefined contacts with a layer of Ti/Au (10/150 nm) remained. Electrical characterization before and after ion beam implantation with argon and aluminum were performed, in order to investigate the impact of ion beam implantation on the electrical and photoconductivity properties, in particular the UV photoresponse increase and the dynamics of the photocurrent decay.

The as-grown samples showed an asymmetric or rectifying behavior, most probably due to the formation of two Schottky contacts with different properties. The focus of further experiments was to determine the thermal stability of the nanowire electric properties at high temperature. Since annealing may influence the electrical properties of the nanowires, one sample was used to study the annealing optimization. Progressive increase of the annealing time results in a larger decrease of the conductivity, indicating increased resistivity of the nanowires.

The as-grown ZnO nanowires were also used to investigate the photoconductivity under different light intensities. It was found that the current increases initial quickly and the increase rate slows down progressively till it saturates. This process can be interpreted in terms of the separation of photogenerated electrons and holes, induced by the surface band bending of the nanowires. Upon both the lowest and highest excitation powers, respectively 20 μW and 5 mW, a decrease of the photocurrent after annealing was observed. The decay of the photoconductivity after UV illumination lasts for several minutes or hours. The recombination of photogenerated charge carriers can be explained in terms of trapping of electrons at the surface, promoted by adsorption of oxygen molecules. With increasing time, the accumulation of electrons at the surface increase the height of the surface potential barrier, which determines a progressive slow down of further electron trapping and therefore a slower photocurrent decay.

Subsequently, the impact of argon implantation on the electrical properties of ZnO nanowires was studied. Argon was found to introduce defects in the crystal lattice without adding additional dopants. SEM images were used for the determination of the changes in morphology after implantation and electrical characterization. A slight reduction in the diameter may be attributed to

the electrical measurements, which lasted in total for several tens of hours. It was shown that the argon implantation on ZnO nanowires lead to a decrease in conductivity even after eight hours annealing. This corresponds to the highly resistive character of the devices due to the large amount of remaining defects. The results concerning the photocurrent decay suggest a decrease in the recovery time, although it was not possible to make a precise comparison since the photocurrents generated by the same excitation intensity differs significantly before and after implantation.

Implantation of aluminum ions in ZnO nanowires can introduce n-type dopants, which contribute to the conductivity. As with argon irradiation, the ion range was again set to 100 nm. SEM investigation before and after aluminum implantation revealed that the implantation process do not induce any significant change in the diameter and do not cause roughness of the surface. Characterization at the probe station directly after implantation revealed poor conductivity due to the presence of defects. However, the current is slightly higher than the non-irradiated nanowire, suggesting that aluminum increases the conductivity of the device. The conductivity increases progressively after each annealing procedure reaching the highest value after 8 hours annealing at 300 °C. Upon annealing, the dopants which are stopped at interstitial positions, after collision with target atoms, diffuse to the substitutional places of zinc. This suggests that thermal annealing is necessary to stimulate diffusion of defects out of the crystal structure and activate the implanted aluminum ions. The photocurrent increase can be attributed to the higher amount of free electrons after substitution of Zn^{2+} ions with Al^{3+} ions which results in a decrease of the depletion width. Comparison of the dynamics before and after aluminum implantation clearly revealed a higher recovery time for the implanted nanowires. The introduction of dopants may be accompanied by the creation of additional defects at the surface. The surface states eventually generated during implantation (sputtering) might cause an increase of the surface band bending, resulting in a larger depletion width and PPC.

The correlation between the electrical properties and the induced defects and dopants was further investigated by performing PL measurements on exact the same ZnO nanowires. The spectra were characterized by near band edge (NBE) emission and deep level emission (DLE) in the visible range. The undoped nanowires show green luminescence that originates from zinc interstitials and oxygen vacancies. The decrease in the ratio between the NBE and the DLE can be attributed to the implantation. The amount of additional implantation induced defects corresponds to the higher intensity of the DLE. The DLE of the implanted samples is a superposition of green and red luminescence. The luminescence in the red band is dominated by excessive oxygen, zinc interstitials and Al^{3+} related donor centers. The NBE emission includes several lines corresponding to bound exciton recombination. According to Schilling et al. [72], the presence of FX is related to high crystal quality; however the decrease in NBE intensity confirms that many defects are still present in the crystal after argon implantation. After aluminum implantation, the PL spectrum is dominated by recombination of bound excitons with aluminum impurity centers. This confirms that the aluminum ions are incorporated in the ZnO nanowire and optical active. In addition to the donor bound exciton transitions, the spectra of undoped and argon doped wires show LO phonon replica and TES transitions, which disappear completely after aluminum implantation. These results suggest that irradiation with aluminum ions influences the emission behavior of the ZnO nanowires.

Having the knowledge of the electrical and optical properties in mind, it is shown that the increase in photocurrent is due to the introduction of n-type dopants. Longer annealing times increase the mobility of the aluminum dopants, which can act as shallow donors and enhances their contribution to the conductivity. The longer recovery time induced by aluminum implantation corresponds to the trapping in deep levels and recombination of electrons and holes, generated by visible excitation [72]. Optical transition between the defects and the band edge correspond to these excitations. The PL spectrum conforms to such optical transition between the defect states.

In conclusion, application of low-dimension systems in industry is still challenging. Although much research has been performed in the past, further efforts are required to improve the understanding and the control of the surface effects. The results obtained during this research contribute to a better understanding of the fundamental procedures. Doping by ion irradiation enables ZnO nanowires to get more favorable properties. Because of the higher surface-to-volume ratio of nanowires, this effect is more pronounced than in bulk materials. This may lead to the development of nanodevices in a better and more effective way with improved performance.

Acknowledgement

I would like to express my sincere gratitude and appreciation to all who helped me in the completion of my master thesis and to those who were a big part of my college life.

To my Professors, especially Hans-Gerd Boyen and Carsten Ronning, for the opportunity to do my thesis in Germany in order to get more inside in the world of science and physics. For their encouragement and undying support, for the guidance towards the right direction and the motivation to become a better scientist. A sincere thank you to Professor Marcel Ameloot to fulfill the function of second examiner and for the follow up of my research progress.

I heartily thank Davide Cammi and Andreas Johannes for the daily supervision. From the first till the last day, I obtained much help. For their patience and answers to all my questions and problems. A big thank you to Robert Röder for performing the PL measurements and the guidance in the interpretation of the results.

To all the members of the research group for welcoming me and giving me the opportunity to experience how it is to become a real scientist. For giving me advice, for the discussions and sharing their experience in the group meeting.

I wish to take this opportunity to express my sincere gratitude to all members of the Institut für Festkörperphysik at the Friedrich-Schiller-University of Jena. I have learned that the best scientific results are always achieved in teamwork, there is no I in team.

Grateful acknowledgement is expressed to my parents Marc and Gerda for motivating me to always do my best in everything. For their hard work to give me the opportunity to study abroad and letting me check one item off my bucket list. For being there for me in times of laughter and when things were not so great, for their undying love and support, for making me feel how proud they are of me. For showing that hard work does pay off and their guidance which made me become the person that I am now.

To my younger brother Philip for all the fun and designing my schemes and figures.

I would also like to thank my friends for always making me smile behind my tears. For their support and the laughter behind the reality of college life, for helping me when I was struggling and for helping me up after every downfall. For showing me what true friendship means.

I hope to see you all soon, either in Belgium or in Germany.
Thank you for being part of my life and my adventures!

Michelle

Danksagung

Ich möchte meinen Dank und Schätzung an alle ausdrücken, die mir bei der Vollendung meiner Masterthesis geholfen haben und an die, die grosser Teil meines College Lebens waren.

An meine Professoren, vor allem Hans-Gerd Boyen und Carsten Ronning, für die Gelegenheit, meine Thesis in Deutschland auszuführen, um tiefer in die Welt der Wissenschaft und Physik einzudringen. Für Ihre Ermutigungen und unendliche Unterstützung, für die Führung in die richtige Richtung und die Motivation, eine bessere Wissenschaftlerin zu werden. Einen herzlichen Dank an Professor Marcel Ameloot, die Funktion des zweiten Prüfers ausgeführt zu haben, und für die Weiterführung der Fortschritte meiner Forschung.

Ich möchte mich bei Davide Cammi und Andreas Johannes für die tägliche Überwachung herzlich bedanken. Von dem ersten bis zu dem letzten Tag habe ich sehr viel Hilfe bekommen. Für Ihre Geduld und Antworten auf alle meine Fragen und Probleme. Ein grosser Dank an Robert Röder für die Leitung der PL Messungen und die Anleitung bei der Interpretation der Ergebnisse.

An alle Mitglieder der Forschungsgruppe, mich willkommen zu haben und mir die Gelegenheit gegeben zu haben, zu erfahren wie es ist, eine richtige Wissenschaftlerin zu werden. Für die Ratschläge, die mir gegeben wurden, für die Diskussionen und ihre Erfahrung in Gruppen-meetings geteilt zu haben.

Ich möchte diese Gelegenheit nutzen, meinen aufrichtingen Dank an alle Mitglieder des Instituts für Festkörperphysik an der Friedrich-Schiller-Universität in Jena auszusprechen. Ich habe gelernt, dass die besten wissenschaftlichen Resultate immer in Team-Arbeit erreicht werden. Es gibt kein Ich in Team.

Dankbare Anerkennung an meine Eltern Marc und Gerda, mich motiviert zu haben, immer mein Bestes in allem zu geben. Für ihre harte Arbeit, mir die Gelegenheit gegeben zu haben, im Ausland zu studieren und eine Sache von meiner Lebenszielliste zu streichen. Dafür immer da für mich gewesen zu sein, in Zeiten des Lachens und auch wenn es mal nicht so einfach war. Für ihre unendliche Liebe und Unterstützung. Dafür mich fühlen zu lassen, wie stolz sie auf mich sind. Dafür gezeigt zu haben, dass harte Arbeit sich ausbezahlt macht und für ihre Leitung, die Person aus mir gemacht zu haben die ich heute bin. An meinen jüngeren Bruder Philip für all den Spass und für das Zeichnen meiner Schemen und Abbildungen.

Ich möchte auch meinen Freunden danken, mich hinter meinen Tränen immer zum Lachen gebracht zu haben. Für ihre Unterstützung und das Lachen hinter der Realität des College-Lebens, für ihre Hilfe, wenn ich gekämpft habe und dafür nach jedem Zusammenbruch aufgeholfen zu haben. Dafür mir gezeigt zu haben, was echte Freundschaft bedeutet.

Ich hoffe, euch alle, entweder in Belgien oder Detuschland, wiederzusehen.
Danke Teil meines Lebens und Abendteuers zu sein!

References

[1] STOREY N. *Electronics, a system approach.* Pearson. 2013.

[2] LI Y., QIAN F., XIANG J. et al. *Nanowire electronic and optoelectronic devices.* Materials today. 2006; 9, 18-27.

[3] VERMEEREN V., WENMACKERS S., WAGNER P., MICHIELS L. *DNA sensors with diamond as a promising alternative transducer material.* Sensors. 2009; 9, 5600-5636.

[4] BAWA R., BAWA R.S., MAEBIUS S.B. et al. *Protecting new ideas and inventions in nanomedicine with patents.* Nanomedicine: Nanotechnology, Biology, and Medicine. 2005; 1, 150-158.

[5] HARTLING T., SEIDENSTICKER A., OLK P. et al. *Controlled photochemical particle growth in two-dimensional ordered metal nanoparticles arrays.* Nanotechnology. 2010; 21, 145309

[6] LOK C. *Nanotechnology: Small wonders.* Nature. 2010; 467, 18-21.

[7] TAYLOR R., OTANICAR T., ROSENGARTEN G. *Nanofluid-based optical filter optimization for PV/T systems.* Light: Science & Applications. 2012; 1, e34.

[8] TIMES E. *IBM sees immersion at 22 nm, and pushes out EUV.* 2007. Available from: http://www.eetimes.com/document.asp?doc_id=1165388

[9] SHARMA P., STREENIVAS K., RAO K.V. *Analysis of ultraviolet photoconductivity in ZnO films prepared by unbalanced magnetron sputtering.* Journal of Applied Physics. 2003; 93, 3963-3970.

[10] SOCI C., ZHANG A., XIANG B. et al. *ZnO nanowire UV photodetectors with high internal gain.* Nano Letters. 2007; 7, 1003-1009.

[11] BAO J., SHALISH I., SU Z. et al. *Photoinduced oxygen release and persistent photoconductivity in ZnO nanowires.* Nanoscale Research Letters. 2011. 6;404

[12] CHEN D., LIU Z., WANG X., SHEN G. *Transparent metal oxide transistors.* Nanoscale. 2012; 4, 3001-3012.

[13] LU J.G., CHANG P., FAN Z. *Quasi-one-dimensional metal oxide materials – synthesis, properties and applications.* Materials Science and Engineering. 2006; 52, 49-91.

[14] MILLER D.R., AKBAR S.A., MORRIS P.A. *Nanoscale metal oxide-based heterojunctions for gas sensing: A review.* Sensors and Actuators B: Chemical. 2014; 204, 250-272.

[15] FAN S.W., SRIVASTAVA A.K., DRAVID V.P. *UV-activated room-temperature gas sensing mechanism of polycrystalline ZnO.* Applied Physics Letters. 2009; 95, 142106.

[16] LI L., YANG H., ZHAO.H et al. *Hydrothermal synthesis and gas sensing properties of single-crystalline ultralong ZnO Nanowires.* Applied PhysicsA. 2010; 98, 635-641.

[17] RONNING C., BORSCHEL C., GEBURT S., NIEPELT R. *Ion beam doping of semiconductor nanowires.* Materials Science and Engineering. 2010; 70, 30-43.

[18] GURNEE E.F. *Fundamental principles of semiconductors.* Journal of Chemical Education. 1969; 46, 80-85.

[19] University of Cambridge. *Metal-Semiconductor Junction – rectifying contact.* Available from: http://www.doitpoms.ac.uk/tlplib/semiconductors/junction_rectifying.php

[20] SZE S.M. *Physics of Semiconductor Devices.* Wiley. 1969.

[21] Tung R.T. *The physics and chemistry of the Schottky barrier height.* Applied Physics Reviews. 2014; 1, 011304.

[22] LITTON C.W., REYNOLDS D.C., COLLINS T.C. *Zinc oxide Materials for electronic and optoelectronic device applications.* Wiley. 2011.

[23] GOLDBERGER J., SIRBULY D.J., LAW M., YANG P. *ZnO nanowire transistors.* Journal of Physical Chemistry B Letters. 2005; 109, 9-14.

[24] WANG S.L. *Zinc oxide nanostructures: growth, properties and applications.* Journal of Physics: Condensed Matter. 2004; 16, 829-858.

[25] AMIN G. *White LEDs printed on paper.* PhD thesis. Quaid-e-Azam University Pakistan. 2012

[26] ÖZGÜR Ü., ALIVOV Y., LIU C. et al. *A comprehensive review of ZnO materials and devices.* Journal of Applied Physics. 2005; 98, 041301.

[27] SMIJS T.G., PAVEL S. *Titanium dioxide and zinc oxide nanoparticles in sunscreens: focus on their safety and effectiveness.* Nanotechnology, Science and Applications. 2011; 4, 95-112.

[28] WANG Z.L., SONG J. *Piezoelectric nanogenerators based on zinc oxide nanowire arrays.* Science. 2006; 312, 242-245.

[29] LIU G., TAM M.C., EI-RAYES K. et al. *Optical and piezoelectric properties of p-type ZnO nanowires on transparent flexible substrate for energy harvesting.* Proc. SPIE. 2014; 9202

[30] LI M., XING G., QUNE L.F.N.A. et al. *Tailoring the charge carrier dynamics in ZnO nanowires: the role of surface hole/electron traps.* Physical Chemistry Chemical Physics. 2012; 14, 3075-3082.

[31] CHEN M.W., RETAMAL J.R.D., CHEN C.Y., HE J.H. *Photocarrier relaxation behavior of a single ZnO nanowire UV photodetector: effect of surface band bending.* IEEE Electron Device Letters. 2012; 30, 411-413.

[32] BESSEGATO G.G., GUARALDO T.T., ZANONI M.V.B. *Enhancement of photoelectrocatalysis efficiency by using nanostructured electrodes.* Nanotechnology and Nanomaterials. 2014; 271-320.

[33] CHEN C.Y., CHEN M.W., KE J.J et al. *Surface effects on optical and electrical properties of ZnO nanostructures.* Pure and Applied Chemistry. 2010; 82, 2055-2073.

[34] MOORE J.C., THOMPSON C.V. *A phenomenological model for the photocurrent transient relaxation observed in ZnO-based photodetector devices.* Sensors. 2013; 13, 9921-9940.

[35] CAMMI D., RONNING C. *Persistent photoconductivity in ZnO nanowires in different atmospheres.* Advances in Condensed Matter Physics. 2014; 184120

[36] LANY S., ZUNGER A. *Anion vacancies as a source of persistent photoconductivity in II-VI and chalcopyrite semiconductors.* Physical Review B. 2005; 72, 035215.

[37] PRADES J.D., HERNANDEZ-RAMIREZ F., JIMENEZ-DIAZ. Et al. *The effects of electron-hole separation on the photoconductivity of individual metal oxide nanowires.* Nanotechnology. 2008; 19, 465501

[38] Thirteenth Ham lesson o' de day. 2011. Available from: http://tymkrs.tumblr.com/post/3525431464/thirteenth-ham-lesson-o-de-day

[39] BORSCHEL C., NIEPELT R., GEBURT S. et al. *Alignment of semiconductor nanowires using ion beam.* Small. 2009; 22, 2576-2580.

[40] BORSCHEL C., NIEPELT R., GEBURT S., RONNING C. *Ion beam doping of semiconductor nanowires.*

[41] RONNING C., BORSCHEL C., GEBURT S. et al. *Tailoring the properties of semiconductor nanowires using ion beams.* Physica Status Solidi B. 2010; 45, 1026-1032.

[42] BORSCHEL C., SPINDLER S., LEROSE D. et al. *Permanent bending and alignment of ZnO nanowires.* Nanotechnology. 2011; 22, 185307.

[43] WAGNER R.S., ELLIS W.C. *Vapor-Liquid-Solid mechanism of single crystal growth.* Applied Physics Letters. 1964; 4, 89-90.

[44] SCHMIDT-MENDE L., MACMAMUS-DRISCOLL J.L. *ZnO-nanostructures, defects, and devices.* Materials Today. 2007; 10, 40-48.

[45] KÄLBLEIN D.D. *Field-effect transistors based on ZnO nanowires.* Phd thesis. École Polytechnique Fédéral de Lausanne. 2011.

[47] LEVINSON H., MCCORD M., RAI-CHOUDHURY P. et al. *Handbook of microlithography, micromachining, and microfabrication.* 1997.

[48] UENO H. *Au wire bonding to Cu pad using Ti thin film.* Japanese Journal of Applied Physics. 1992; 31, 1547-1548.

[49] KEITHLEY INSTRUMENTS INC. *Electrical characterization of carbon nanotube transistors (CNT FETs) with the model 4200-SCS semiconductor characterization system.* Application note series. 2010.

[50] SWAPP S. *Scanning electron microscopy.* University of Wyoming.

[51] High Voltage Engineering Europa. Available from: http://www.highvolteng.com/

[52] ZIEGLER J.F., BIERSACK J. P., LITTMARK U. *The Stopping and Range of Ions in Matter.* Pergamon. 1985.

[53] ZIEGLER J. *Particle interactions in matter.* 2011.

[54] BORSCHEL C., SPINDLER S., LEROSE D. et al. *Permanent bending and alignment of ZnO nanowires.* Nanotechnology. 2011; 22, 185307.

[55] LU G.J., CHANG P., FAN Z. *Quasi-one-dimensional metal oxide materials – Synthesis, properties and applications.* Materials Science and Engineering. 2006; 52, 49-91.

[56] BERA A., GHOSH T., BASAK D. et al. *Enhanced photoluminescence and photoconductivity of ZnO nanowires with sputtered Zn.* ACS Applied Materials and Interfaces. 2010. 2; 2898-2903.

[57] SUNDARAM K.B., KHAN A. *Work function determination of zinc oxide films.* Journal of Vacuum Science and Technology A. 1997. 15; 428-430.

[58] CORNIL D., VAN REGEMORTER T., BELJONNE D., CORNIL J. *Work function shifts of a zinc oxide surface upon deposition of self-assembled monolayers: a theoretical insight.* Physical Chemistry Chemical Physics. 2014. 16; 20887-20899.

[59] HÖLZL J., SCHULTE F.K. *Work functions of metals.* Solid Surface Physics. 1979.

[60] AWAD M.A., IBRAHIM E.M.M., AHMED A.M. *Synthesis and thermal stability of ZnO nanowires.* Journal of Thermal Analysis and Calorimetry. 2014; 117, 635-642.

[61] SUBANNAJUI K., KIM D.S., ZACHARIAS M. *Electrical analysis of individual ZnO nanowires.* Journal of Applied Physics. 2008; 104, 014308.

[62] MAHMOOD A., AHMED N., RAZA Q. *Effect of thermal annealing on the structural and optical properties of ZnO thin films deposited by the reactive e-beam evaporation technique.* Physica Scripta. 2010; 82, 065801.

[63] GEBURT S. *Lasing and ion beam doping of semiconductor nanowires.* PhD thesis. Friedrich-Schiller-Universität Jena. 2013.

[64] KURIBARA K., WANG H., UCHIYAMA N. *Organic transistors with high thermal stability for medical applications.* Nature Communications. 2012; 3, 1-7.

[65] SHARMA P., SREENIVAS K. RAO K.V. *Analysis of ultraviolet photoconductivity in ZnO films prepared by unbalanced magnetron sputtering.* Journal of applied Physics. 2003; 93, 3963-3970.

[66] LI W.Q., XIAO X.H., STEPANOV A.L. et al. *The ion implantation-induced properties of one-dimensional nanomaterials.* Nanoscale Research Letters. 2013; 8, 175.

[67] JOHANNES A. *In-situ characterization of ion-doped zinc oxide nanowires.* Masterthesis. Friedrich-Schiller-Universität Jena. 2011.

[68] RONNING C., GAO P.X., DING Y. et al. *Manganese-doped ZnO nanobelts for spintronics.* Applied Physics Letters. 2004. 84; 783-785.

[69] JAYANTHI K., CHAWLA S. *Electronic and luminescent characteristics of aluminum doped ZnO nanocrystals. Electronic Material Letters.* 2015. 11; 55-59.

[70] CHEN Y.Y., WANG P.W., HSU J., LEE C. *Post-annealing properties of aluminum-doped zinc oxide films fabricated by ion beam co-sputtering.* Vacuum. 2013. 87; 227-231.

[71] CHAUHAN R.N., ANAND R.S., KUMAR J. *RF-sputterend Al-doped ZnO thin films: Optoelectrical properties and application in photovoltaic devices.* Physica Status Solidi A. 2014. 11; 2514-2522.

[72] SCHILLING M., HELBIG R., PENSL G. *Bound exciton luminescence of Ar- and Al-implanted ZnO.* Journal of Luminescence. 1985. 33; 201-212.

[73] WANG X., ZHANG P., HONG R. *Preparation and application of aluminum-doped zinc oxide powders via precipitation and plasma processing method.* Journal of Applied Polymer Science. 2015. 22; 41990.

[74] WESCH W, WENDLER E, SCHNOHR C.S. *Damage evolution and amorphization in semiconductors under ion irradiation.* Nuclear Instruments and Methods in Physics Research Section B. 2012. 277; 58-69.

[75] VANHEUSDEN K., SEAGER C.H., WARREN W.L. et al. *Correlation between photoluminescence and oxygen vacancies in ZNO phosphors.* Applied Physics Letters. 1996; 68, 403-405.

[76] DJURISIC A.B., LEUNG Y.H., TAM K.H. et al. *Defect emissions in ZnO nanostructures.* Nanotechnology. 2007; 18, 095702.

[77] MOORE J.C., THOMPSON C.V. *A phenomenological model for the photocurrent transients relaxation observed in ZnO-based photodetector devices.* Sensors. 2013; 113, 9921-9940.

[78] HUANG M.H., WY Y., FEICK H. et al. *Catalytic growth of zinc oxide nanowires by vapor transport.* Advanced Materials. 2001. 13; 113-116.

[79] ALVI N.H., HASAN K.UK, NUR O., WILLANDER M. *The origin of the red emission I nn-ZnO nanotubes/p-GaN white light emitting diodes.* Nanoscale Research Letters. 2011; 6, 130.

[80] WILLANDER M., NUR O., SADAF J.R. et al. *Luminescence from zinc oxide nanostructures and polymers and their hybrid devices.* Materials. 2010; 3, 2643-2667.

[81] MEYER B.K., ALVES H., HOFMANN D.M. et al. *Bound exciton and donor-acceptor pair recombinations in ZnO.* Physica Status Solidi B. 2004; 241, 231-260.

Auteursrechtelijke overeenkomst

Ik/wij verlenen het wereldwijde auteursrecht voor de ingediende eindverhandeling:
Ion beam doping and defect engineering of ZnO nanowires for photodetection and sensing applications

Richting: **master in de biomedische wetenschappen-bio-elektronica en nanotechnologie**
Jaar: **2015**

in alle mogelijke mediaformaten, - bestaande en in de toekomst te ontwikkelen - , aan de Universiteit Hasselt.

Niet tegenstaand deze toekenning van het auteursrecht aan de Universiteit Hasselt behoud ik als auteur het recht om de eindverhandeling, - in zijn geheel of gedeeltelijk -, vrij te reproduceren, (her)publiceren of distribueren zonder de toelating te moeten verkrijgen van de Universiteit Hasselt.

Ik bevestig dat de eindverhandeling mijn origineel werk is, en dat ik het recht heb om de rechten te verlenen die in deze overeenkomst worden beschreven. Ik verklaar tevens dat de eindverhandeling, naar mijn weten, het auteursrecht van anderen niet overtreedt.

Ik verklaar tevens dat ik voor het materiaal in de eindverhandeling dat beschermd wordt door het auteursrecht, de nodige toelatingen heb verkregen zodat ik deze ook aan de Universiteit Hasselt kan overdragen en dat dit duidelijk in de tekst en inhoud van de eindverhandeling werd genotificeerd.

Universiteit Hasselt zal mij als auteur(s) van de eindverhandeling identificeren en zal geen wijzigingen aanbrengen aan de eindverhandeling, uitgezonderd deze toegelaten door deze overeenkomst.

Voor akkoord,

Geelen, Michelle

Datum: **8/06/2015**